HHS Public Access

Author manuscript

Circ Res. Author manuscript; available in PMC 2021 February 14.

Published in final edited form as:

Circ Res. 2020 February 14; 126(4): 417–435. doi:10.1161/CIRCRESAHA.119.316241.

TRIC-A Channel Maintains Store Calcium Handling by Interacting with Type 2 Ryanodine Receptor in Cardiac Muscle

Xinyu Zhou[1,*], **Ki Ho Park**[1,*], **Daiju Yamazaki**[2], **Pei-hui Lin**[1], **Miyuki Nishi**[2], **Zhiwei Ma**[3], **Liming Qiu**[3], **Takashi Murayama**[4], **Xiaoqin Zou**[3], **Hiroshi Takeshima**[2], **Jingsong Zhou**[5], **Jianjie Ma**[1]

[1]Department of Surgery, Davis Heart and Lung Research Institute, The Ohio State University, Columbus, OH 43210;

[2]Department of Biological Chemistry, Kyoto University Graduate School of Pharmaceutical Sciences, Kyoto, Japan;

[3]Department of Physics and Astronomy, Dalton Cardiovascular Research Center, Department of Biochemistry, University of Missouri, Columbia, MO 65211;

[4]Department of Pharmacology, Juntendo University School of Medicine, Tokyo, Japan;

[5]College of Nursing and Health Innovation, University of Texas at Arlington, Arlington, TX 76019

Abstract

Rationale: TRIC-A and TRIC-B are distributed to endoplasmic reticulum (ER)/sarcoplasmic reticulum (SR) intracellular Ca^{2+} stores. The crystal structure of TRIC has been determined, confirming the homo-trimeric structure of a potassium channel. While the pore architectures of TRIC-A and TRIC-B are conserved, the carboxyl-terminal tail domains (CTT) of TRIC-A and TRIC-B are different from each other. Aside from its recognized role as a counter-ion channel that participates in excitation-contraction coupling of striated muscles, the physiological function of TRIC-A in heart physiology and disease has remained largely unexplored.

Objective: In cardiomyocytes, spontaneous Ca^{2+} waves, triggered by store overload-induced Ca^{2+} release (SOICR) mediated by the type 2 ryanodine receptor (RyR_2), develop extra-systolic contractions often associated with arrhythmic events. Here we test the hypothesis that TRIC-A is a physiologic component of RyR_2-mediated Ca^{2+} release machinery that directly modulates SOICR activity via CTT.

Methods and Results: We show that cardiomyocytes derived from the TRIC-$A^{-/-}$ mice display dysregulated Ca^{2+} movement across SR. Biochemical studies demonstrate a direct interaction between CTT-A and RyR_2. Modeling and docking studies reveal potential sites on RyR_2 that show differential interactions with CTT-A and CTT-B. In HEK293 cells with stable expression of RyR_2, transient expression of TRIC-A, but not TRIC-B, leads to apparent suppression of spontaneous

Address Correspondence to: Dr. Jianjie Ma, Department of Surgery, The Ohio State University Wexner Medical Center, 460 West 12th Avenue, Columbus, OH 43210, Tel. 614-292-2636, Jianjie.Ma@osumc.edu.

*XZ and KHP contributed equally to this manuscript.

DISCLOSURES

None.

Ca^{2+} oscillations. Ca^{2+} measurements using the cytosolic indicator Fura-2 and the ER luminal store indicator D1ER suggest that TRIC-A enhances Ca^{2+} leak across the ER by directly targeting RyR_2 to modulate SOICR. Moreover, synthetic CTT-A peptide facilitates RyR_2 activity in lipid bilayer reconstitution system, enhances Ca^{2+} sparks in permeabilized TRIC-$A^{-/-}$ cardiomyocytes, and induces intracellular Ca^{2+} release after microinjection into isolated cardiomyocytes, whereas such effects were not observed with the CTT-B peptide. In response to isoproterenol stimulation, the TRIC-$A^{-/-}$ mice display irregular electrocardiogram and develop more fibrosis than the WT littermates.

Conclusions: In addition to the ion-conducting function, TRIC-A functions as an accessory protein of RyR_2 to modulate SR Ca^{2+} handling in cardiac muscle.

Graphical Abstract

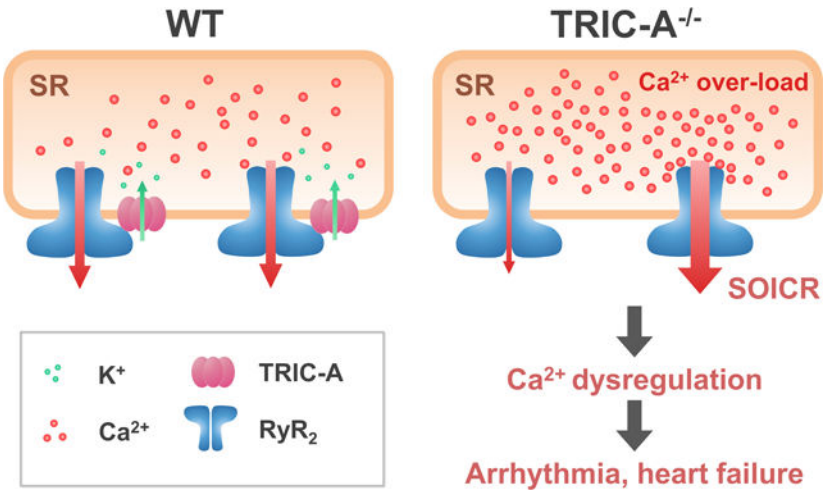

TRIC channels were discovered in 2007. Aside from its recognized role as a counter-ion channel, the physiological function of TRIC-A in the heart has remained largely unexplored. Even with the recent resolution of the crystal structure of the TRIC channels, the interacting partners for TRIC have yet to be defined. This study uncovered a novel function for TRIC-A as an accessory protein that interacts with the RyR to modulate intracellular Ca^{2+} release in cardiomyocytes. The CTT domain of TRIC-A, an important portion of the channel that is left out of the crystal structure determination, constitutes an active motif that interacts with RyR. The vulnerability of the TRIC-A knockout mouse heart to handling of isoproterenol stimulation further support the important physiological function of TRIC-A in heart physiology and disease.

Keywords

RYR2 gene; calcium signaling; excitation-contraction coupling; SOICR; TMEM38a

Subject Terms:

Basic Science Research; Calcium Cycling/Excitation-Contraction Coupling; Myocardial Biology

INTRODUCTION

In cardiac muscle, sarcolemma depolarization triggers the release of Ca^{2+} from the sarcoplasmic reticulum (SR) via Ca^{2+}-induced Ca^{2+} release (CICR)[1–3]. During this process, Ca^{2+} influx through the voltage-dependent Ca^{2+} channels on the sarcolemma activates the type 2 ryanodine receptor (RyR_2) channel located on the SR. Under certain pathological conditions, spontaneous Ca^{2+} release from the SR can take place in the absence of membrane excitation due to store overload induced Ca^{2+} release (SOICR)[4–10]. SOICR may evoke propagating Ca^{2+} waves that can further result in delayed after-depolarizations, which may cause arrhythmias in heart failure.

The SR Ca^{2+} store of cardiomyocytes is maintained by uptake and release processes, both of which are electrogenic events. The release of Ca^{2+} through the RyR_2 channels will lead to the development of a negative potential inside the SR lumen, and this would further limit Ca^{2+} release from the SR if uncompensated. Likewise, SERCA-mediated uptake of Ca^{2+} into the SR would lead to the accumulation of a positive potential within the SR lumen, and that would tend to inhibit Ca^{2+}-pumping function. Thus coordinated counter-ion movements are required to balance the SR membrane potential in order to maintain efficient Ca^{2+} release and uptake in cardiomyocytes.

In 2007, Takeshima and colleagues identified trimeric intracellular cation (TRIC) channels located on the SR and endoplasmic reticulum (ER) of multiple cell types[11]. In human and mouse genomes, two isoforms of TRIC genes were identified: TRIC-A, a subtype predominantly expressed in SR of excitable cells, and TRIC-B, a ubiquitous subtype expressed in ER of all tissues[11–21]. TRIC-A and TRIC-B appear to have different functions in Ca^{2+} signaling in excitable and non-excitable cells, since knocking out TRIC-B affects IP_3 receptor mediated Ca^{2+} release in airway epithelial cells, which results in respiratory defects and neonatal death with TRIC-$B^{-/-}$ pups[21]. The TRIC-$A^{-/-}$ mice, in addition to dysfunction of skeletal muscle[20], develop hypertension that is linked to defective Ca^{2+} sparks and spontaneous transient outward currents in arterial smooth muscle[19]. A common feature with the TRIC-$A^{-/-}$ and TRIC-$B^{-/-}$ mice is the development of Ca^{2+} overload inside the SR/ER of multiple tissues[11, 19–21]. This Ca^{2+} overload can impact the function of SOICR, causing instability of Ca^{2+} movement across the SR membrane in muscle cells, which could further contribute to tissue dysfunctions associated with ablation of the TRIC genes.

While researchers over the past ten years have established that genetic ablations or mutations of TRIC channels are associated with hypertension, muscle dysfunction, respiratory defects, and brittle bone disease[11–21], the function of TRIC channels in heart physiology and disease has yet to be established. El-Ajouz et al[22] reported dampened activity of RyR channels in skeletal muscle lacking TRIC-A, suggesting TRIC-A could play a modulatory role in control of RyR-mediated intracellular Ca^{2+} release. Recently, the crystal structure of TRIC has been determined, confirming the homo-trimeric structure of a potassium channel[23–26]. While the pore architectures of TRIC-A and TRIC-B appear to be conserved, the carboxyl-terminal tail (CTT) domains of TRIC-A and TRIC-B are different from each other. These CTT domains

show the flexible structure and potentially interfere with crystal formation, thus all available structural determinations of the TRIC channels were obtained without the CTT domain.

Here we report that cardiomyocytes derived from the TRIC-A$^{-/-}$ mice show dysregulated Ca^{2+} movement across the SR membrane. Our biochemical and immunohistochemical studies show that TRIC-A can physically associate with RyR_2 via the CTT domain. Reconstitution studies in the lipid bilayer membrane, Ca^{2+} measurements in adult cardiomyocytes and heterologous cells demonstrate that TRIC-A, in addition to serving as a counter-ion channel, can interact with RyR_2 to modulate the intracellular Ca^{2+} homeostasis and consequently the operation of SOICR.

METHODS

The data, analytical methods, and other study materials will be provided upon reasonable request to the corresponding author.

Cardiomyocyte isolation from adult mice.

TRIC-A knock out (TRIC-A$^{-/-}$) mice used in this study were reported in our previous publication[11]. Handling of mice followed IACUC guidelines from The Ohio State University. Isolated hearts from adult TRIC-A$^{-/-}$ and wild type (WT) littermate mice (10–12 weeks of both genders) were perfused with a Langendorff apparatus at 37°C. The enzyme digestion step consisted of perfusing Tyrode's solution containing 1 mg/ml collagenase (Type II, 300 U/mg; Worthington) and 0.1 mg/ml protease (Type XIV) for 6 min. Cardiomyocytes were dissociated from digested ventricles by gentle mechanical dissociation and used within 3 hours. The Tyrode's solution contained (in mM) 136 NaCl, 5.4 KCl, 0.33 NaH_2PO_4, 1.0 $MgCl_2$, 10 glucose and 10 HEPES (pH 7.4).

Mice and isoproterenol-treatment protocol.

Alzet mini-osmotic pump (Alza Corp.) containing either isoproterenol (ISO), phosphate-buffered saline (PBS) as a control were surgically inserted subcutaneously in mice under isoflurane anesthesia. The mini-osmotic pump provides controlled delivery of ISO (60 mg/kg/day). In separate study, 80 mg/kg ISO was injected once intraperitoneally in mice under isoflurane anesthesia. 1 hour later, electrocardiogram (ECG) was measured using Animal Bio Amp and PowerLab 8/30, and analyzed by LabChart 7.0 (ADInstruments).

Hearts from the TRIC-A$^{-/-}$ and WT mice were collected at the indicated times after ISO treatment, fixed in 10% formalin-containing PBS, and embedded in paraffin. Serial 4-μm heart sections were cut and stained with H & E and Masson's trichrome. Blinding was not performed because the genotype of mice was already known before the experiments were conducted.

Ca^{2+} sparks and waves measurement in cardiomyocytes.

Intracellular Ca^{2+} sparks of intact cardiomyocytes isolated from adult mouse (4–8 months age) were recorded using a Zeiss780 confocal microscope with a 40× 1.42 NA oil immersion objective. Cardiomyocytes were loaded with Fluo-4-AM (2 μM) and then

stimulated with a field stimulation of 0.5 Hz for 20 seconds in a normal Tyrode's solution containing 1.8 mM Ca^{2+}. Spontaneous Ca^{2+} spark activities were measured afterward. Experiments were conducted at room temperature (24–26 °C).

Isolated cardiomyocytes were loaded with 5 μM Fluo-4 AM (Thermo Fisher Scientific) in 1.8 mM Ca^{2+} physiological salt solution (PSS) (in mM): 130 NaCl, 5.6 KCl, 1 $MgCl_2$, 11 glucose, and 10 Hepes, pH 7.4 for 30 min at room temperature. Line scan images of Fluo-4 fluorescence intensity were acquired at a sampling rate of 2 ms per line using the Galvano scan mode of a Nikon A1R confocal microscope. During the 1 min line scan imaging, cardiomyocytes were subjected to an electric field stimulation of 0.2 Hz, 10 ms duration pulses of 6 V.

To examine the impact of store-overload induced intracellular Ca^{2+} release in the isolated cardiomyocytes, extracellular Ca^{2+} was increased from 1.8 mM to 10 mM in PSS containing 50 μM BTS to mitigate myocyte contraction. Serial x-y images of cardiomyocytes in 10 mM Ca^{2+} PSS were acquired at 130 ms per frame using the resonant scan mode of Nikon A1R confocal microscope. All image data were analyzed by Fiji-ImageJ.

Separate studies were performed with Ca^{2+} spark measurement in saponin-permeabilized cardiomyocytes, following the protocol of Lukyanenko and Gyorke[27] and Guo et al[28]. Specifically, cardiomyocytes were permeabilized with saponin (0.01% for ~45 s). The MaxChelator program (URL: maxchelator.stanford.edu) developed by Bers et al[29] was used to prepare the solution for precise control of free cytosolic Ca^{2+}. The cytosolic solution contained (mM): 120 potassium aspartate, 5 MgATP, 10 phosphocreatine, 0.03 Fluo-4 pentapotassium salt, 10 Hepes (pH 7.25) and 5 U/ml creatine phosphokinase, with 0.4 EGTA and 0.087 $CaCl_2$ which buffers free Ca^{2+} at 100 nM. The Fluo-4 dye was excited with the 488 nm line of a LED laser (0.30% of maximum power, Nikon-A1R), pinhole 2.0 (equivalent to 39.6 μm). The use of low laser-power avoids laser-induced damage to cardiomyocytes during line-scan imaging of Ca^{2+} sparks using the Nikon-A1R imaging system. During Ca^{2+} spark measurement, 0.001% saponin was continuously present in the cytosolic solution to avoid resealing of the sarcolemmal membrane. Quantification and characterization of Ca^{2+} sparks were performed using SparkMaster ImageJ program[30].

Plasmid construction.

The mouse TRIC-A or TRIC-B cDNA was cloned into pCMS-mRFP vector (Clontech). The pCMS-mRFP plasmid contained a red fluorescent protein (RFP) reporter gene driven under a separate SV40 promoter, allowing for selection of cells transfected with TRIC-A or TRIC-B using red fluorescence. For the investigation of the carboxyl-terminal tail (CTT) domain of TRIC on Ca^{2+} signaling, two chimeras were constructed, TRIC-AB and TRIC-BA. TRIC-AB contains a.a. 1–230 from TRIC-A plus a.a. 229–291 from TRIC-B. TRIC-BA contains a.a. 1–228 from TRIC-B plus a.a. 231–299 from TRIC-A. The cDNA coding sequences were chemically synthesized (Quintara Biosciences, CA) and cloned into the pCMS-mRFP vector to express the chimeric TRIC proteins in mammalian cells. All plasmid identities were confirmed by gene sequencing.

Baculovirus production and its infection to HEK293 cells.

Baculovirus carrying vesicular stomatitis virus G-protein (VSVG) on the virus envelope that effectively infects mammalian cells was produced as described previously[31]. cDNAs for TRIC-A and TRIC-B were cloned into the modified pFastBac1 vector (Invitrogen). Baculovirus was produced in Sf9 cells according to the manufacturer's instructions (Invitrogen). P2 virus was used for the experiments. HEK293 cells inducibly expressing RyR_2 which were kindly provided by Dr. Nagomi Kurebayashi or control HEK293 cells were cultured in DMEM, 5% FBS, 1% penicillin, and streptomycin at 37°C, 5% CO_2. P2 virus solution was supplemented to the culture media to infect the virus and cells were observed at 36 hours post infection.

Ca^{2+} imaging in HEK293 cells.

HEK293 cells with inducible expression of RyR_2 were provided by Dr. Wayne Chen and cultured in DMEM, 5% FBS, 1% penicillin, and streptomycin at 37°C, 5% CO_2[5]. pCMS-mRFP plasmids containing the various TRIC-A and TRIC-B cDNAs were transfected into HEK293 cells using lipofectamine reagent following manufacture's instruction. 24 hours later, tetracycline (0.1 μg/ml) was added to the culture medium to induce RyR_2 expression. Measurements of cytosolic Ca^{2+} were conducted at 16–18 hours post tetracycline induction. Cells were loaded with Fura-2-AM (5 μM) or Fluo-4 AM (2 μM) in 0 Ca^{2+} Krebs–Ringer Hepes (KRH) buffer containing (mM): 125 NaCl, 5 KCl, 25 HEPES, 6 glucose, and 1.2 $MgCl_2$, pH 7.4 for 40 min at room temperature. All solutions were prepared with double-distilled H_2O (18.2 MΩ cm resistance). Cells were then continuously perfused with KRH solution containing different concentrations of $CaCl_2$ (0–2.0 mM) at room temperature. Fura-2 fluorescence was captured by a dual-wavelength excitation spectrofluorometer (Photon Technology International, Monmouth Junction, NJ) with fast switching of 340 nm and 380nm excitations. Fluorescence of Fluo-4 was excited at 488 nm and detected by a Zeiss 780 confocal microscope.

In separate studies, HEK-293 cells with inducible expression of RyR_2 were co-transfected with TRIC-A and D1ER cDNA, or TRIC-B and D1ER to determine the impact of TRIC-A/TRIC-B on the ER Ca^{2+} stores. Cells were perfused continuously at room temperature with KRH containing 2 mM $CaCl_2$. Tetracaine (2 mM) was used to block RyR_2 activity, and caffeine (10 mM) was used to activate RyR_2 to deplete the ER Ca^{2+} store. Cells were excited at 458 nm, and emissions of yellow fluorescent protein (YFP) and cyan fluorescent protein (CFP) from D1ER were captured every 0.5 s. The amount of fluorescence resonance energy transfer (FRET) was determined by the ratio of the emissions at 535 and 480 nm[5, 32].

Immunoblotting.

HEK293 cells expressing RyR_2 and TRIC-A were harvested and lysed in RIPA buffer (50 mM Tris-HCl pH 7.4, 150 mM NaCl, 1% Triton x-100, 1% sodium deoxycholate, 0.1% SDS, 1 mM EDTA) supplemented with a protease inhibitor cocktail (PIC, Sigma) for 10 min at 4°C. PIC contains (final concentration) AEBSF (1 mM), aprotinin (0.8 μM), bestatin (40 μM), E-64 (14 μM), leupeptin (20 μM) and pepstatin A (15 μM). Heart lysates derived from wild type mouse were used for positive control of TRIC-A and RyR_2. Mouse hearts were minced and re-suspended in PIC containing RIPA buffer. Heart protein extraction was done

by three-cycle of freeze-thawing on dry ice and extracted with pestle homogenizer with disposable polypropylene pestles (Thermo Fisher Scientific). Cells or tissue lysates were centrifuged (20,000 × g, 15 min. at 4°C) and protein containing supernatant was collected. Protein concentration was determined using a Bio-Rad Protein Assay kit. 10 μg of protein were loaded on 12% or 5% SDS-PAGE and transferred onto a polyvinylidene difluoride membrane for detection of TRIC-A or RyR_2 expressions, respectively. The expression levels of TRIC-A or RyR_2 were visualized using specific antibodies anti-RyR_2 (34C) (1:3000) (Abcam, ab2868) and anti-TRIC-A (1:2000) (Proteintech Group, 19920–1-AP).

Immunofluorescence staining.

Isolated mouse cardiomyocytes were washed by phosphate buffered saline (PBS) and fixed in 4% phosphate-buffered paraformaldehyde (PFA) for 20 min at room temperature, and then permeabilized for 15 min with 0.2% Triton X-100 in PBS. Cells were blocked by 3% BSA for 40 min and then incubated with TRIC-A (Proteintech Group, 19920–1-AP) and RyR_2 antibodies (1:200, Abcam, ab2868) at 4°C overnight. Alexa 647 labeled goat anti-rabbit (Thermo Fischer A21244) and Alexa 546 labeled goat anti-mouse (Thermo Fisher A11003) secondary antibodies were applied and incubated for 1 h at 37 °C. After a brief wash, DAPI was used to stain the nucleus for 5 min and then washed by PBST 5 times. TRIC-$A^{-/-}$ mice heart was used as negative control for TRIC-A antibody and IgG only staining was used for RyR_2 antibody staining that confirmed the specificity of both antibodies. Images were captured by Zeiss LSM 780 confocal microscope and analyzed by ImageJ.

GST-CTT-A protein expression and beads binding assay.

cDNA coding for the CTT domain of TRIC-A (a.a. 231–299) was cloned into the pGEX4T-1 bacteria expression plasmid. The pGEX-CTT-A plasmid was transformed into *E. coli* (DH5α), and expression of GST-CTT-A protein was induced with 0.3 mM isopropyl-β-D-thiogalactopyranoside (IPTG, Sigma) for 3.5 h at 30°C. Harvested bacterial pellets were re-suspended in a buffer containing 20 mM Tris-HCl, 200 mM NaCl, and 0.2 mM PMSF (pH 7.5) supplemented with 0.5% protease inhibitor cocktails (PIC, Sigma), 1 mg/ml lysozyme, and 1 mg/ml $MgCl_2$, and sonicated (Branson Ultrasonics) for 15 s for 5 cycles at 30% power output. The lysates were centrifuged twice at 15,000 rpm for 30 min at 4°C. The cleared supernatants were diluted 1:4 into the suspension buffer, mixed with Glutathione Sepharose Beads (Amersham) and incubated at 4°C overnight on an orbital shaker. The mixture was then loaded into a poly-prep chromatography column (Bio-Rad), allowed to precipitate by gravity, and then washed with 50 ml buffer containing 20 mM Tris-HCl, 200 mM NaCl, 0.2 mM PMSF and PIC, pH 7.5. C1148 cells with stable expression of RyR_1 were described previously[33, 34]. Microsomal vesicles derived from C1148 cells or SR vesicles derived from rat heart (kindly provided by Dr. Michael Fill, Rush University, Chicago) were lysed in RIPA buffer supplemented with PIC, and loaded to either GST or GST-CTT-A bound beads and incubated at 4°C on an orbital shaker for 3 hours. The bound proteins were washed 4 times with buffer containing 0.5% NP-40, 20 mM Tris (pH 7.4) supplemented with PIC, eluted with sample loading buffer, and loaded onto SDS-PAGE gel and western blotted with anti-RyR (1:3000, Abcam, ab2868).

Channel activity assay on planar bilayer system.

SR vesicles isolated from rat hearts were used for lipid bilayer reconstitution studies of single RyR_2 channels[35, 36]. The SR vesicles were kindly provided by Dr. Michael Fill at Rush Medical University[28]. Planar lipid bilayers were formed with a lipid composition of phosphatidylethanolamine and phosphatidylserine (Avanti Polar Lipids, Birmingham, AL) (1:1 ratio, dissolved in decane, 50 mg/ml) across a 200 μm diameter hole in a polystyrene partition. CTT-A and CTT-B peptides were synthesized by GL Biochem (Shanghai, China) with >95% purity. SR vesicles and CTT-A or CTT-B peptides were added to one chamber using *cis* design, composed of 250 mM CsCl, 0.22 mM $CaCl_2$, 1 mM EGTA, 10 mM HEPES, pH 7.4. The other chamber, designated as *trans*, contained 50 mM CsCl, 10 mM HEPES, pH 7.4. Single channel data acquisition and analysis were conducted with pClamp software.

Microinjection of CTT-A and CTT-B peptide.

CTT-A and CTT-B peptides were dissolved in PBS solution at a concentration of 10 μM. Freshly isolated wild type mouse cardiomyocytes were loaded with 5 μM Fluo-4 AM. Microinjection pipettes made of borosilicate glass (Sutter Instrument Co.) were prepared using a micropipette puller (Model P-97, Sutter Instrument Co.). The microfilament inside the pipette ensures that the solution reaches the tip for microinjection. The tip pore of the pipette was adjusted to allow for delivery of 10–20 pico liter of peptide solution in 60 ms using a picospritzer (Parker Instrumentation) coupled to PatchMan micromanipulator (Eppendorf). Changes in intracellular $[Ca]_i$ were monitored under a BioRad confocal microscope.

Modeling and Docking of CTT-A and CTT-B with RyR_2.

The atomic structures of CTT-A and CTT-B, were modeled using the I-TASSER server[37]. The atomic structure of human RyR_2 ($hRyR_2$) has not been solved. However, the cryo-EM structures of porcine RyR_2 ($pRyR_2$) are available in the Protein Data Bank[38] (PDB ID: 5goa, open state; PDB ID: 5go9, closed state)[39]. Due to the large size of RyR_2, traditional homology modeling cannot be used to model human RyR_2 using $pRyR_2$ structures. Instead, mutations were introduced in the structures of $pRyR_2$ (5goa and 5go9, respectively) following the $hRyR_2$ sequence, using UCSF Chimera[40]. The structures of CTT-A and CTT-B were respectively docked onto the homology model of $hRyR_2$ using our in-house docking software, MDockPP[41, 42]. The P1 domain, P2 domain, and channel domain were blocked from docking to reduce the enormous search space on the huge RyR_2 protein, as the peptides unlikely interact with these domains. Four potential binding sites of CTT-A/CTT-B were identified, and the representative binding mode in each site was optimized using the minimization tool of UCSF Chimera to remove intermolecular side chain clashes. The differential binding modes in the binding sites were further compared between the open and closed state of the $hRyR_2$ channel.

Data handling and statistical analysis.

D'Agostino & Pearson normality test was used to evaluate normality of the data. If normal, we used unpaired t-test for single comparison and Tukey's test for multiple comparisons. If

not normal, we used non-parametric test (Mann-Whitney test for single comparison or Dunn's test for multiple comparisons) to derive the p-value. Before doing a Tuckey's or Dunn's test for multiple comparisons, ANOVA or Kruskal-Wallis (if not passed normality test) test was conducted for the whole group.

Data are represented as mean ± standard deviation. A value of $P<0.05$ was considered significant. All data were analyzed using Excel and Prism 8 software.

RESULTS

Abnormal Ca^{2+} signaling in cardiomyocytes derived from the TRIC-$A^{-/-}$ mice.

We have generated knockout mice carrying the deletion of either *TRIC-A* or *TRIC-B*. While TRIC-$A^{-/-}$ mice survived past their adolescent age, homozygous ablation of *TRIC-B* proved lethal as the *TRIC-*$B^{-/-}$ mice died at the neonatal stage due to respiratory dysfunction[21]. Moreover, the aggravated embryonic fatality was observed with the *TRIC-*$A^{-/-}$*TRIC-*$B^{-/-}$ mice, demonstrating the essential role of TRIC in development[11, 17]. Using cardiomyocytes derived from the TRIC-$A^{-/-}$ adult mice and littermate wild type (WT) controls (10–12 weeks age), we examined Ca^{2+} spark signaling properties following electrical pacing. As shown in Fig. 1A, following a 0.5 Hz electrical field stimulation for 20 s, spontaneous Ca^{2+} sparks were observed in the isolated cardiomyocytes upon the termination of the electric stimulation. Compared with the WT cardiomyocytes, the TRIC-$A^{-/-}$ cardiomyocytes showed less frequent Ca^{2+} sparks (Fig. 1B, *left*). Interestingly, the amplitudes of individual Ca^{2+} sparks appear to be significantly higher in TRIC-$A^{-/-}$ cardiomyocytes than those in WT cardiomyocytes (Fig. 1B, *middle*).

We also compared caffeine-induced Ca^{2+} release from the WT and TRIC-$A^{-/-}$ cardiomyocytes. As illustrated in (Fig. 1B, *right*), the total caffeine-releasable Ca^{2+} pool from the SR was significantly higher in TRIC-$A^{-/-}$ than in WT cardiomyocytes. This observation is consistent with our published data with skeletal muscle[20] and epithelial cells[21] where the absence of TRIC-A or TRIC-B led to elevated Ca^{2+} storage inside the SR or ER.

Confocal line scan imaging of Fluo-4 fluorescence revealed different patterns of intracellular Ca^{2+} transients in WT and TRIC-$A^{-/-}$ cardiomyocytes following electric field stimulation (Fig. 1C). There appeared to be a delayed onset of intracellular Ca^{2+} transients and a prolonged decaying phase of Ca^{2+} transients in the TRIC-$A^{-/-}$ cardiomyocytes compared with those in the WT cardiomyocytes. On average, the rising time of Ca^{2+} transients was significantly longer in TRIC-$A^{-/-}$ cardiomyocytes when compared with WT cardiomyocytes (Fig. 1D). The full-duration-half-maximal (FDHM) of Ca^{2+} transients was significantly longer in the TRIC-$A^{-/-}$ cardiomyocytes (Fig 1E), whereas the amplitude of Ca^{2+} transients showed no significant difference (Fig. 1F) between the WT and TRIC-$A^{-/-}$ cardiomyocytes. Studies from other investigators demonstrated that reduced RyR_2 channel activity could contribute to the delayed time-to-peak and prolonged decaying phase of electric pacing-induced Ca^{2+} release from cardiomyocytes[43–45]. This suggests the possibility that ablation of TRIC-A in cardiomyocytes could lead to reduced function of the RyR_2 channel.

Using the resonant scan mode of the Nikon A1R confocal microscope, we performed continuous x-y imaging of spontaneous Ca^{2+} waves (at a rate of 130 ms per frame) in the isolated cardiomyocytes upon elevation of the extracellular Ca^{2+} from 1.8 mM to 10 mM. Such fast time-lapse imaging enabled us to examine the impact of TRIC-A ablation on the speed of Ca^{2+} wave propagation. As shown in Fig. 1G, the speed of Ca^{2+} wave propagation appeared to be faster in WT than in TRIC-$A^{-/-}$ cardiomyocytes (see Online Movie I and II). Measurements from multiple experiments support the statistical difference in the speed of Ca^{2+} wave propagation between WT and TRIC-$A^{-/-}$ cardiomyocytes (Fig. 1H). Moreover, the percentage of cells that displayed Ca^{2+}-overload induced spontaneous Ca^{2+} waves was significantly lower in TRIC-$A^{-/-}$ cardiomyocytes than that in WT cardiomyocytes (Fig. 1I). In Online Movie III and IV, one could see the different behavior of Ca^{2+} waves in WT and TRIC-$A^{-/-}$ cardiomyocytes.

Isoproterenol treatment induces irregular ECG and cardiac fibrosis in TRIC-$A^{-/-}$ mice.

Under basal condition, there was no clear difference in electrocardiograms (ECG) recorded in the TRIC-$A^{-/-}$ mice and WT littermates (Fig. 2A). However, following a bolus intraperitoneal injection of isoproterenol (ISO, 80 mg/kg), irregular ECG was observed with the TRIC-$A^{-/-}$ mice at 1 hour post ISO injection, whereas the WT mice displayed regular patterns of ECG. Analysis of the R-R intervals between the individual ECGs demonstrated large variations, confirming the irregularity of ISO-induced ECG with the TRIC-$A^{-/-}$ mice (Fig. 2B).

We next tested if ablation of TRIC-A could alter the response of the mice to chronic treatment with ISO. With chronic treatment of ISO (60 mg/kg/day for 2 weeks, delivered using an Alzet mini-osmotic pump), the TRIC-$A^{-/-}$ heart would develop extensive fibrosis than the WT heart (Fig. 2C). Mason's trichrome staining revealed significant increase in fibrosis in the heart tissue derived from the TRIC-$A^{-/-}$ mice at 2 weeks post ISO treatment, compared with the WT mice (Fig. 2D).

Thus, chronic exposure to ISO likely caused increased death of cardiomyocytes and fibrotic remodeling, which may be linked to the overload of SR Ca^{2+} associated with ablation of TRIC-A. In response to ISO, SR Ca^{2+} overload may cause mitochondria Ca^{2+} toxicity and apoptosis in the TRIC-$A^{-/-}$ cardiomyocytes. Further dissecting the role of TRIC-A in modulating the Ca^{2+} signaling crosstalk from SR to mitochondria will require dedicated effort in future studies.

Co-expression of TRIC-A and RyR_2 in HEK293 cells modulates SOICR.

We used HEK293 cells with tetracycline-inducible expression of RyR_2 to investigate the impact of TRIC-A and TRIC-B on RyR_2-mediated intracellular Ca^{2+} signaling[5, 6] (Fig. 3A). In this model, the elevation of extracellular $[Ca]_o$ lead to increased Ca^{2+} content inside the ER, which triggered the opening of the RyR_2 channel via its luminal Ca^{2+} sensing mechanism, leading to the appearance of SOICR. Previously, we showed that co-expression of RyR_1 and MG29 in Chinese hamster ovary (CHO) cells caused depletion of the ER Ca^{2+} store and consequently apoptotic cell death[46]. Interestingly, we found that transient co-expression of RyR_2 and TRIC-A, but not TRIC-B, in HEK293 cells led to changes in cell

morphology, and a large portion of the cells expressing TRIC-A and RyR_2 would die within 36 hours (Fig. 3B), suggesting cytotoxicity by potential perturbation of ER Ca^{2+} homeostasis.

For assaying the effect of TRIC-A in HEK293 cells, we used a dual-reporter plasmid with mRFP-expression cassette driven by a separate promoter. This allows selection of transfected vs non-transfected cells in the same dish (Fig. 3C). From the line-scan measurements, it is clear that cells co-expressing RyR_2 and TRIC-A (red labeled) did not show oscillating patterns of Ca^{2+} signaling, unlike those cells expressing RyR_2 alone, which often display Ca^{2+} oscillations. A representative trace of Ca^{2+} measurement in a HEK293 cell with co-expression of TRIC-A and RyR_2 (labelled red, Fig. 3D), illustrates the apparent absence of spontaneous Ca^{2+} oscillations. After treatment of tetracaine, a RyR_2 blocker, SOICR was diminished and cytosolic Ca^{2+} level was decreased. At the end of the recording, caffeine was introduced to the dish to test the release of Ca^{2+} via RyR_2. Ca^{2+} release from TRIC-A transfected cells triggered by caffeine confirmed the apparent suppression of SOICR is not due to the dysfunction of RyR_2 (Fig. 3D, *top*). This effect appears to be specific to TRIC-A, as co-expression with TRIC-B did not affect RyR_2-mediated SOICR in HEK293 cells (Fig. 3D, *bottom*). Summary data from multiple experiments is shown in Fig. 3E, indicating that TRIC-A, not TRIC-B, could modulate SOICR in HEK293 cells.

Studies from Chen and colleagues demonstrated that the frequency of RyR_2-mediated SOICR in HEK293 cells was dependent on the concentration of Ca^{2+} in the extracellular solution[5]. Here we tested if co-expression of TRIC-A and RyR_2 could modulate SOICR in a Ca^{2+}-dependent manner. The data shown in Fig. 3F clearly suggest that the presence of TRIC-A could alter $[Ca]_o$-dependent activation of SOICR. Moreover, this effect is TRIC-A specific, since cells with co-expression of TRIC-B and RyR_2 showed similar response as those transfected with vector alone (as control).

To elucidate the mechanism of TRIC-A mediated modulation of SOICR, we used D1ER, a Ca^{2+} biosensor targeted to ER, to directly measure ER luminal Ca^{2+} level[5, 32, 47]. We followed the approach developed by Bers and colleagues to assay the ER Ca^{2+} content using tetracaine to inhibit RyR_2 activity[48, 49]. This will allow for testing to what extent co-expression of TRIC-A alters the Ca^{2+} leak rate across the ER. As shown in Fig. 4A, HEK293 cells co-expressing RyR_2 and TRIC-A displayed reduced ER Ca^{2+} content (measured with the D1ER probe), when compared with cells expressing RyR_2 alone. While cells expressing RyR_2 alone show oscillating patterns of ER Ca^{2+} content (Fig. 4A, *blue trace*) that mirrors the SOICR signal (Fig. 4B), co-expression with TRIC-A led to apparent suppression of the ER Ca^{2+} content below the oscillating threshold levels (Fig. 4A, *red trace*). In addition, we observed less Ca^{2+} release by direct caffeine treatment in TRIC-A expressing cells (Fig. 4B). This data further supports that TRIC-A reduced the ER Ca^{2+} content in the RYR_2 expressing HEK293 cells.

The effect of TRIC-A on ER Ca^{2+} handling likely require the participation of the RyR_2 channel, since transfection of TRIC-A in HEK293 cells (in the absence of RyR_2) did not affect the ER Ca^{2+} content as measured by ATP-induced Ca^{2+} release through IP_3R (Fig. 4C) nor cytotoxicity (Fig. 3B). Moreover, when blocking ER Ca^{2+} uptake by cyclopiazonic

acid (CPA), the decline of luminal Ca^{2+} is not affected by TRIC-A (Fig. 4D). These results support that altered ER Ca^{2+} signaling by TRIC-A is RyR_2 dependent.

TRIC-A interact with RyR_2 through its carboxyl-terminal tail (CTT) domain.

We performed immunohistochemical (IHC) staining of TRIC-A and RyR_2 in cardiomyocytes derived from the WT mice. The clear overlap between TRIC-A and RyR_2 could be observed (Fig. 5A). Images were analyzed by Pearson and Manders coefficients and showed significant co-localization (Fig. 5B).

Topology analysis revealed that both TRIC-A and TRIC-B contained large CTT domains that reside in the cytosol (Fig. 5C). This CTT domain likely represents a flexible structure that interfered with crystallization and thus was not included in the structural determination of TRIC channels by Liu and colleagues[50]. The CTTs of TRIC-A and TRIC-B diverge from each other. CTT-A contains a histidine-rich motif and a polylysine domain that are flanked by a hydrophobic domain. This structure is similar to the intracellular loop joining repeats II and III of the L-type Ca^{2+} channel, which has been shown to be a critical domain that regulates the activity of the SR Ca^{2+} release in muscle cells[51–53]. Only the polylysine domain appears in the CTT-B domain.

To test if the divergent CTT-A constitutes a site for interaction with the RyR channel, we generated a GST-fusion peptide containing the CTT-A (a.a. 231–299) and CTT-B (a.a. 229–291). These recombinant peptides were purified from *E. coli* as GST-fusion proteins. Using a protein pull-down assay, we observed that CTT-A could interact with RyR_1 stably expressed in CHO cells[54, 55] (Fig. 5D), and RyR_2 from rat heavy SR vesicles (Fig. 5E). Using antibodies against RyR_2, we could co-immunoprecipitate TRIC-A from HEK293 cells that co-express RyR_2 and TRIC-A (Fig. 5F). These interactions appear to be specific for CTT-A, as GST peptide alone could not pull down either RyR_1 or RyR_2. In addition to RyR_2, several other candidate proteins were pulled-down by CTT-A as marked by ***a, b*** and ***c*** in Fig. 5E. MALDI-MS identification revealed a-band contains SERCA, MPP1, and C2CD2; b-band contains TRIC-A, destrin, Rtn2, and proteolytic fragment derived from RyR_2; and the c-band contains mostly proteolytic fragment for RyR_2 and SERCA.

TRIC-A carboxyl-terminal tail peptide increases RyR_2 channel activity.

Based on these findings, we generated chimeric constructs of TRIC-AB or TRIC-BA. TRIC-AB contains a.a. 1–230 from TRIC-A plus a.a. 229–291 from TRIC-B. TRIC-BA contains a.a. 1–228 from TRIC-B plus a.a. 231–299 from TRIC-A. These constructs were co-expressed with RyR_2 in HEK293 cells. We found that replacement of the CTT domain in TRIC-A with CTT-B could alleviate the impact on SOICR (Fig. 6). Consistent with the data shown in Fig. 3, co-expression of TRIC-A with RyR_2 could reduce the spontaneous Ca^{2+} oscillation in HEK293 cells (Fig. 6A, red color), whereas co-expression of TRIC-B with RyR_2 had no effect on SOICR activity (Fig. 6A, green color). Co-expression of TRIC-AB with RyR_2 resulted in the elimination of the inhibitory effect of TRIC-A on SOICR (Fig. 6A, orange color). This finding supports the important function of CTT-A on RyR_2-mediated SOICR in HEK293 cells. Interestingly, co-expression of TRIC-BA with RyR_2 also had minimal effect on RyR_2-mediated SOICR (Fig. 6B, blue color), suggesting the

possibility that CTT-A alone in the context of TRIC-B might lose its capability to interact with the RyR_2 channel.

We used 10 mM caffeine to induce activation of the RyR_2 channel as the assessment of the total ER Ca^{2+} load (Fig. 6C). Clearly, only TRIC-A had a significant impact on the caffeine response, whereas TRIC-B, TRIC-AB and RIC-BA had a negligible effect on ER Ca^{2+} content in HEK293 cells expressing RyR_2.

For direct evaluation of the CTT-A and CTT-B peptides on RyR_2 channel function, we reconstituted the RyR_2 channels from rat cardiac muscle into the lipid bilayer membrane. As shown in Fig. 6D, the addition of CTT-A to the cis-cytoplasmic solution significantly enhanced the RyR_2 channel activity (n=5). The effect appears to be specific for CTT-A, as the addition of CTT-B peptide did not result in significant changes in RyR_2 channel activity (n=4). Data from multiple experiments are summarized in Fig. 6F.

To further evaluate the functional effect of CTT-A and CTT-B peptides on Ca^{2+} signaling in cardiomyocytes, we performed microinjection of CTT-A or CTT-B peptides into isolated mouse cardiomyocytes (Fig. 6E). We found that microinjection of CTT-A peptide elicited significantly more intracellular Ca^{2+} events as compared to those cardiomyocytes injected with CTT-B peptide (Fig. 6G).

CTT-A modulates Ca^{2+} spark activity in cardiomyocytes derived from TRIC-$A^{-/-}$ cardiomyocytes.

We followed the protocol of Lukyanenko and Gyorke[27] to characterize the Ca^{2+} spark activity in saponin-permeabilized cardiomyocytes derived from wild type and TRIC-$A^{-/-}$ mice (Fig. 7A). Saponin permeabilization of the sarcolemma allows access of CTT-A and CTT-B to the intracellular organelles of the cardiomyocytes. Starting from a basal condition of 100 nM free Ca^{2+} in the cytosolic solution, we observed the significantly lower frequency of spontaneous Ca^{2+} sparks in the TRIC-$A^{-/-}$ cardiomyocytes compared with the wild type cardiomyocytes (Fig. 7B). For testing the effect of CTT-A or CTT-B on Ca^{2+} spark signaling, the free cytosolic Ca^{2+} was reduced to 50 nM, which led to lower activity of Ca^{2+} spark events in the TRIC-$A^{-/-}$ cardiomyocytes (Fig. 7C). When CTT-A (10 μM) was added to the cytosolic solution, transient elevation of Ca^{2+} spark activity was observed in the early phase (within 3 min after CTT-A addition), which is followed by a decline of Ca^{2+} spark activity during the later phase (starting from ~3 min following CTT-A addition) (Fig. 7C, *left*). In the presence of CTT-A, we frequently observed Ca^{2+} spark events that occur in a consecutive streaming pattern of opening-closings, reflecting increased RyR_2 channel activity. Such streaming patterns of Ca^{2+} spark events were rarely observed under control conditions and did not appear to change with either early or late treatment of CTT-B (10 μM) (Fig. 7C, *right*). Diary plot of Ca^{2+} spark activity over the 10 min time period remained steady under the control condition of 50 nM free Ca^{2+} in the cytosol (Fig. 7D, *left*). Clearly, the addition of CTT-A led to transient stimulation of the spontaneous Ca^{2+} spark events (Fig 7D, *middle*). In contrast, CTT-B did not have a measurable impact on Ca^{2+} spark activity (Fig 7D, *right*). Data from multiple experiments were summarized in Fig. 7E, showing a significant increase in CTT-A-induced transient Ca^{2+} spark activity which did not occur with CTT-B. Consistent with the streaming pattern of Ca^{2+} spark events observed with CTT-A

treatment that may cause depletion of the SR Ca^{2+} store (Fig. 7C, *left*), quantitative analysis revealed significant reduction of Ca^{2+} spark amplitude in the presence of CTT-A, but not CTT-B (Fig. 7F). The effect of CTT-A on Ca^{2+} sparks measured from the saponin-permeabilized cardiomyocytes derived from in the TRIC-$A^{-/-}$ mice is reversible, as washout of CTT-A led to the recovery of Ca^{2+} spark activities to the basal level (Supplemental Online Figure I).

CTT-A and CTT-B dock to different motifs on RyR_2.

To gain insights into the interaction of CTT-A or CTT-B with the RyR_2 channel, we performed modeling and docking studies using our established molecular dynamic simulation method[37]. We first compared the 3-D structure of CTT-A with CTT-B and found divergent structural patterns between the two peptides (Fig. 8A). Interestingly, the close similarity between CTT-A and the II-III loop peptide of the dihydropyridine receptor (DHPR) was observed (Fig. 8B).

Molecular docking of CTT-A and CTT-B onto the human RyR_2 ($hRyR_2$) showed four potential binding sites, which were numbered according to their rankings by the energy scoring function in MDockPP[56]. Representative binding modes of CTT-A at these four sites on the closed structure of $hRyR_2$ are plotted in Fig. 8C. Among them, Site 1 and Site 2 exist in both open and closed structures of $hRyR_2$ for both CTT-A and CTT-B. Site 1, the best ranked site, is the hinge domain of $hRyR_2$[39], which has been shown to play a critical role in the activation of the RyR_2 channel. Site 2 consists of binding domain with FKBP12 (see PDB ID: 3J8H[57]), which has demonstrated function in control of RyR channel opening. The zoom-in picture of CCT-A interacting with the closed structure of $hRyR^2$ is shown in Supplemental Online Fig. II.

Interestingly, CTT-A and CTT-B bind distinctively on Site 3 and Site 4 (Fig. 8D). Site 3 locates on the N-terminal domain (NTD), and Site 4 locates on the SPRY domain. CTT-A binds to Site 3 for both the open and closed state of $hRyR_2$, whereas CTT-B binds to Site 3 only for the closed state of $hRyR_2$. CTT-A binds to Site 4 only in the closed state, whereas CTT-B binds to Site 4 only in the open state. Previous studies by Tae et al showed that the SPRY domain of RyR potentially contributes to binding to DHPR for control of RyR channel activity[58]. While our modeling study suggested conformation-dependent interaction of CTT-A with the SPRY domain, further biochemical and structure-function studies will be required to test if the modeled CTT-A/SPRY interaction or CTT-A's binding to other domains of RyR_2 indeed play a role in the control of Ca^{2+} release from the SR.

DISCUSSION

The present study uncovered a novel function for TRIC-A as an accessory protein that interacts with RyR_2 to modulate intracellular Ca^{2+} signaling. Aside from its recognized role as a counter-ion channel that participates in excitation-contraction coupling of striated muscles, the physiological function of TRIC-A in heart physiology and disease has remained largely unexplored. Even with the recent resolution of the crystal structure of the TRIC channels, the interacting partners for TRIC have yet to be defined. We showed that CTT of TRIC-A, an important portion of the channel that is left out of the crystal structure

determination, constitutes an active motif that interacts with RyR_2 to control SOICR function. We found that TRIC-B is ineffective in control of RyR_2-mediated SOICR in cultured cells, suggesting the specificity of TRIC-A interaction with the RyR_2 channel. Using reconstitution studies and Ca^{2+} spark measurements, we demonstrated that the synthetic CTT-A peptide could directly enhance the RyR_2 channel activity and stimulate intracellular Ca^{2+} release in isolated cardiomyocytes.

While many studies have suggested that altered function of SOICR from the SR in cardiomyocytes may contribute to the development of cardiac arrhythmias[32, 47, 59–61], searching for accessory proteins that modulate RyR_2 channel function and SR Ca^{2+} homeostasis should yield important clues to the function of SOICR in physiological and pathophysiological settings. We showed that TRIC-A ablation led to SR Ca^{2+} overload, yet the spontaneous Ca^{2+} sparks and store-overload induced Ca^{2+} waves were less frequent in cardiomyocytes derived from the TRIC-$A^{-/-}$ mice compared with those from the WT mice. Moreover, such SR Ca^{2+} overload did not trigger SOICR in the TRIC-$A^{-/-}$ cardiomyocytes under basal conditions. Through the determination of the ER Ca^{2+} content, we showed that overexpression of TRIC-A could increase Ca^{2+} leak across the ER in HEK293 cells. The TRIC-A mediated increase of ER Ca^{2+} leak reflects direct activation of the RyR_2 channel, for expression of TRIC-A alone in the absence of RyR_2 did not affect ER Ca^{2+} storage or passive Ca^{2+} leak across the ER. From these studies, we conclude that TRIC-A constitutes a physiological component of the SR Ca^{2+} release machinery, and TRIC-A deficiency could render RyR_2 channels less sensitive to physiological activation of Ca^{2+} signaling in cardiac muscle. The vulnerability of the TRIC-A knockout mouse heart to handling of isoproterenol stimulation further support the important physiological function of TRIC-A in heart physiology and disease.

It is known that changes in RyR_2 activity can impact the frequency, as well as the speed of stress-induced Ca^{2+} waves in cardiomyocytes. Studies from other investigators have shown that experimental manipulations or mutagenesis of the RyR_2 channel that caused reduction of the RyR_2 channel activity led to slower onset and prolonged decaying phase of voltage-induced Ca^{2+} transients and reduced speed of Ca^{2+} wave propagation[43–45]; and conversely mutations of RyR_2 (e.g. R4496C) that enhance RyR_2 channel activity had the opposite effect on intracellular Ca^{2+} transients[62]. Moreover, Ca^{2+} wave velocity increased with treatment of caffeine and decreased with treatment of tetracaine or flecainide[62]. Ullrich et al[63] reported that cardiomyocytes expressing RyR_2-S2808A displayed slower Ca^{2+} wave velocity. Our data demonstrated that cardiomyocytes derived from the TRIC-$A^{-/-}$ mice displayed reduced frequency of Ca^{2+} sparks and reduced speed of Ca^{2+} wave propagation, likely reflecting reduced RyR_2 activity. When cardiomyocytes are exposed to a high Ca^{2+} (10 mM) extracellular solution, less frequent store-overload induced Ca^{2+} waves were observed in the TRIC-$A^{-/-}$ cardiomyocytes than those in the WT cardiomyocytes. Moreover, the frequency of stress-induced Ca^{2+} waves was less in the TRIC-$A^{-/-}$ cardiomyocytes than that in the WT cardiomyocytes. Following electric pacing, there was a delayed onset of intracellular Ca^{2+} transients and prolonged decaying phase of Ca^{2+} transients in the TRIC-$A^{-/-}$ cardiomyocytes compared with those in the WT cardiomyocytes. Similar observations were also made by other investigators who reported extended decay of Ca^{2+} transients in cardiomyocytes derived from the A4860G mice (with reduced RyR_2 activity)[45] and from the

RyR_2-Ex3-$del^{+/-}$ mice[44], indicating that alteration of RyR_2 activity alone would impact the decaying phase of intracellular Ca^{2+} transient. However, the apparent delayed phase of intracellular Ca^{2+} release from the TRIC-$A^{-/-}$ cardiomyocytes may involve additional actions on other components of Ca^{2+} uptake and release across the SR, e.g. counter-ion movement or SERCA activity. While our data support the notion that alteration of RyR_2 activity associated with genetic ablation of TRIC-A could be a main contributing factor for the dysfunctional intracellular Ca^{2+} signaling in cardiomyocytes, we could not rule out the possibility that changes in SERCA activity could also contribute to the altered Ca^{2+} handling in the TRIC-$A^{-/-}$ cardiomyocytes.

Smith and O'Neill[64] described the effect of low ATP and tetracaine on spontaneous Ca^{2+} waves in permeabilized cardiomyocytes. Lower ATP was shown to cause reduced frequency and slower Ca^{2+} wave propagation, and the changes in Ca^{2+} wave characteristics in 0.5 mM ATP were similar to those observed during perfusion with 50 μM tetracaine. Smith and O'Neill[64] also reported that the SR Ca^{2+} content increased as ATP was reduced or tetracaine was increased. Both tetracaine and lowering ATP are known to cause reduction of the RyR_2 channel activity. Many features of the changes in Ca^{2+} sparks and Ca^{2+} waves reported by Smith and O'Neill[64] are very similar to what we observed with the TRIC-$A^{-/-}$ cardiomyocytes. This further support the notion that ablation of TRIC-A leads to reduced RyR_2 activity in cardiomyocytes.

A recent study from Sitsapesan and colleagues found that in skeletal muscle, the RyR_1 channel from the TRIC-$A^{-/-}$ mice displays increased sensitivity to Mg^{2+} inhibition, defective response to protein kinase A phosphorylation, and physiological activator such as ATP is less effective in activating the individual RyR_1 channels reconstituted into the lipid bilayer membrane[22]. They also reported that the Ca^{2+}-dependent control of RyR_1 channel was not altered in the absence of TRIC-A, suggesting that the modulatory effect of TRIC-A may involve other factors. These findings are consistent with a potential role of TRIC-A as an enhancer of RyR channels, such that the absence of TRIC-A leads to reduced RyR channel function under stress conditions.

Crystal structures of several TRIC channels from invertebrate and prokaryotic TRIC channels have been reported[23–26]. All of these TRIC proteins share very similar folding and trimeric organizations. Interestingly, all of these crystal structures lack the highly flexible CTT domain, which investigators claim may decrease the stability of the crystal[23–26]. Our findings that TRIC-A directly modulates RyR_2-mediated SOICR may have wide implications in cardiovascular research. Potential therapeutic interventions can be used to target the functional interaction between TRIC-A and RyR_2 to restore defective Ca^{2+} signaling in cardiovascular diseases.

In our studies testing CTT-A on Ca^{2+} sparks measured in permeabilized cardiomyocytes, we found an interesting phenomenon. The stimulatory effect of CTT-A on Ca^{2+} sparks was transient, and there appeared to be a delayed inhibitory effect on Ca^{2+} sparks with prolonged incubation of CTT-A. The transient increase in Ca^{2+} sparks induced by CTT-A may reduce the SR Ca^{2+} content that would reduce the frequency of Ca^{2+} sparks after the CTT-A stimulation, or alternatively the inhibitory effect of CTT-A likely reflected other components

of Ca^{2+} movement across the SR membrane. Since the functional effect on intracellular Ca^{2+} release was only observed with CTT-A, not CTT-B, differential interaction between RyR_2 and CTT-A would be required. Using the available information about the 3-D structure of the RyR_2 channel[39], we performed modeling and docking studies and discovered potential sites of interaction between RyR_2 and CTT-A/CTT-B. Of the four sites plotted in Fig. 8C (see also Supplemental Online Fig. II), one of them is particularly interesting. The SPRY domain of RyR_2 constitutes a potential binding site (site 4) for interaction with CTT-A and CTT-B. CTT-A preferentially accesses the SPRY domain when the channel is in the closed state, whereas CTT-B appears to recognize the SPRY domain when the channel is in the open state. Several studies have demonstrated that the SPRY domain of RyR plays an important role in modulation of the Ca^{2+} release channel activity[58, 65]. It should be emphasized that our modeling studies only provide a hint of possible domain-domain interaction between CTT-A/B and RyR. Further mutagenesis studies will be required to ascertain the functional impact of such interaction in control of intracellular Ca^{2+} release in muscle cells.

Previous studies from Chen and colleagues showed that reconstitution of RyR_2 gain-of-function mutants in HEK293 cells could lead to enhanced SOICR as reflected by increased Ca^{2+} oscillations and/or reduced threshold of luminal Ca^{2+} to trigger Ca^{2+} oscillations[5, 6, 59, 66]. Interestingly, our study revealed that co-expression of TRIC-A and RyR_2 led to an apparent reduction of Ca^{2+} oscillation in HEK293 cells, which seems unexpected based on the role of TRIC-A as an enhancer of RyR_2 function. In fact, when TRIC-A was introduced into HEK293 cells, increased Ca^{2+} leak across the ER was observed that may reflect direct activation of the RyR_2 channel. It is possible that the TRIC-A/RyR_2-mediated ER Ca^{2+} leak may take place in the form of small Ca^{2+} release events which are un-synchronized and therefore do not appear as Ca^{2+} oscillations. One would ask why TRIC-A would lead to over activation of RyR_2 in HEK293 cells but not in native cardiomyocytes. It is known that coordinated activation and inactivation mechanisms must exist in cardiomyocytes for the proper function of Ca^{2+} signaling in the heart, and many of the stabilizers or inhibitory factors of RyR_2-mediated Ca^{2+} release are likely absent in HEK293 cells. One avenue of future study may take advantage of HEK293 cells to reconstitute the potential functional interaction of TRIC-A with other regulatory components of the intracellular Ca^{2+} release machinery. Our data support the dual function of TRIC-A as a counter-ion channel and an activator of RyR_2, and both functions would enhance RyR_2-mediated Ca^{2+} release in cardiac muscle. A direct interaction between TRIC-A and RyR_2 constitutes an important physiologic component of intracellular Ca^{2+} signaling in the heart. Studies from Fill and colleagues suggested that due to the non-selective nature of the Ca^{2+} release channels, RyR channels can provide a certain extent of counter currents by themselves[28, 67, 68]. Quantitative simulations suggested that TRIC channels could contribute to the network of SR membrane potential to support Ca^{2+} release and reuptake[68]. Thus, in addition to regulating the acute phase of Ca^{2+} release from the SR/ER store, TRIC-mediated movement of counter current flow could also play a role in balancing the electronegative influence of Ca^{2+} release on other aspects of Ca^{2+} homeostasis inside the SR/ER.

TRIC-A and TRIC-B have different functions in regulating SR and ER Ca^{2+} homeostasis in excitable and non-excitable cells, respectively[11, 16–21]. TRIC-B is present in both excitable

and non-excitable cells, whereas TR-A is predominantly expressed in excitable tissues such as striated muscles and brain tissues. We showed that the divergent CTT domains of TRIC-A and TRIC-B have different functions in modulation of RyR_2 channel activity. Previously we have demonstrated that epithelial cells derived from the TRIC-B knockout mice display abnormal function of IP_3 receptor (IP_3R) mediated Ca^{2+} release from the ER store[21], and skeletal muscle derived from the TRIC-A knockout mice display abnormal function of RyR_1-mediated Ca^{2+} release from the SR store[20]. The functional crosstalk between IP_3R and RyR-mediated Ca^{2+} signaling has been implicated in muscle and heart cells under physiologic and pathologic conditions[69–75]. Dissecting the function of TRIC-A and TRIC-B in modulating RyR/IP_3R cross-talk for control of Ca^{2+} signaling in health and disease will be an important task of future research.

Supplementary Material

Refer to Web version on PubMed Central for supplementary material.

ACKNOWLEDGMENTS

We thank Dr. S.R Wayne Chen for critical reading of this manuscript. We also thank Dr. Michael Fill for providing the cardiac SR vesicles for the biochemical and lipid-bilayer reconstitution studies, and Dr. Lianbo Yu for help with the statistical analysis.

SOURCES OF FUNDING

This work is supported by NIH grants to J. Ma, J. Zhou and JSPS Core-to-Core Program, JSPS Bilateral Open Partnership Joint Research Projects to HT.

Nonstandard Abbreviations and Acronyms:

SR	sarcoplasmic reticulum
CICR	Calcium induced Calcium release
SOICR	store overload induced calcium release
ECG	electrocardiogram
RyR	ryanodine receptor
TRIC	trimeric intracellular cation channels
CTT	carboxyl-terminal tail
CPA	cyclopiazonic acid

REFERENCES

1. Bers DM. Cardiac excitation-contraction coupling. Nature. 2002;415:198–205. [PubMed: 11805843]
2. Cannell MB and Kong CH. Local control in cardiac E-C coupling. J Mol Cell Cardiol. 2012;52:298–303. [PubMed: 21586292]

3. Bround MJ, Asghari P, Wambolt RB, Bohunek L, Smits C, Philit M, Kieffer TJ, Lakatta EG, Boheler KR, Moore ED, Allard MF and Johnson JD. Cardiac ryanodine receptors control heart rate and rhythmicity in adult mice. Cardiovasc Res. 2012;96:372–80. [PubMed: 22869620]
4. Priori SG and Chen SR. Inherited dysfunction of sarcoplasmic reticulum Ca2+ handling and arrhythmogenesis. Circ Res. 2011;108:871–83. [PubMed: 21454795]
5. Jiang D, Xiao B, Yang D, Wang R, Choi P, Zhang L, Cheng H and Chen SR. RyR2 mutations linked to ventricular tachycardia and sudden death reduce the threshold for store-overload-induced Ca2+ release (SOICR). Proc Natl Acad Sci U S A. 2004;101:13062–7. [PubMed: 15322274]
6. Jiang D, Wang R, Xiao B, Kong H, Hunt DJ, Choi P, Zhang L and Chen SR. Enhanced store overload-induced Ca2+ release and channel sensitivity to luminal Ca2+ activation are common defects of RyR2 mutations linked to ventricular tachycardia and sudden death. Circ Res. 2005;97:1173–81. [PubMed: 16239587]
7. Fabiato A Two kinds of calcium-induced release of calcium from the sarcoplasmic reticulum of skinned cardiac cells. Adv Exp Med Biol. 1992;311:245–62. [PubMed: 1529757]
8. Lakatta EG. Functional implications of spontaneous sarcoplasmic reticulum Ca2+ release in the heart. Cardiovasc Res. 1992;26:193–214. [PubMed: 1423412]
9. Marban E, Robinson SW and Wier WG. Mechanisms of arrhythmogenic delayed and early afterdepolarizations in ferret ventricular muscle. J Clin Invest. 1986;78:1185–92. [PubMed: 3771791]
10. Orchard CH, Eisner DA and Allen DG. Oscillations of intracellular Ca2+ in mammalian cardiac muscle. Nature. 1983;304:735–8. [PubMed: 6888540]
11. Yazawa M, Ferrante C, Feng J, Mio K, Ogura T, Zhang M, Lin PH, Pan Z, Komazaki S, Kato K, Nishi M, Zhao X, Weisleder N, Sato C, Ma J and Takeshima H. TRIC channels are essential for Ca2+ handling in intracellular stores. Nature. 2007;448:78–82. [PubMed: 17611541]
12. Yamazaki D, Yamazaki T and Takeshima H. New molecular components supporting ryanodine receptor-mediated Ca(2+) release: roles of junctophilin and TRIC channel in embryonic cardiomyocytes. Pharmacol Ther. 2009;121:265–72. [PubMed: 19095005]
13. Zhao X, Yamazaki D, Kakizawa S, Pan Z, Takeshima H and Ma J. Molecular architecture of Ca2+ signaling control in muscle and heart cells. Channels (Austin). 2011;5:391–6. [PubMed: 21712647]
14. Weisleder N, Takeshima H and Ma J. Immuno-proteomic approach to excitation--contraction coupling in skeletal and cardiac muscle: molecular insights revealed by the mitsugumins. Cell Calcium. 2008;43:1–8. [PubMed: 18061662]
15. Pitt SJ, Park KH, Nishi M, Urashima T, Aoki S, Yamazaki D, Ma J, Takeshima H and Sitsapesan R. Charade of the SR K+-channel: two ion-channels, TRIC-A and TRIC-B, masquerade as a single K+-channel. Biophys J. 2010;99:417–26. [PubMed: 20643059]
16. Zhao C, Ichimura A, Qian N, Iida T, Yamazaki D, Noma N, Asagiri M, Yamamoto K, Komazaki S, Sato C, Aoyama F, Sawaguchi A, Kakizawa S, Nishi M and Takeshima H. Mice lacking the intracellular cation channel TRIC-B have compromised collagen production and impaired bone mineralization. Sci Signal. 2016;9:ra49. [PubMed: 27188440]
17. Zhou X, Lin P, Yamazaki D, Park KH, Komazaki S, Chen SR, Takeshima H and Ma J. Trimeric intracellular cation channels and sarcoplasmic/endoplasmic reticulum calcium homeostasis. Circ Res. 2014;114:706–16. [PubMed: 24526676]
18. Tao S, Yamazaki D, Komazaki S, Zhao C, Iida T, Kakizawa S, Imaizumi Y and Takeshima H. Facilitated hyperpolarization signaling in vascular smooth muscle-overexpressing TRIC-A channels. J Biol Chem. 2013;288:15581–9. [PubMed: 23592776]
19. Yamazaki D, Tabara Y, Kita S, Hanada H, Komazaki S, Naitou D, Mishima A, Nishi M, Yamamura H, Yamamoto S, Kakizawa S, Miyachi H, Yamamoto S, Miyata T, Kawano Y, Kamide K, Ogihara T, Hata A, Umemura S, Soma M, Takahashi N, Imaizumi Y, Miki T, Iwamoto T and Takeshima H. TRIC-A channels in vascular smooth muscle contribute to blood pressure maintenance. Cell Metab. 2011;14:231–41. [PubMed: 21803293]
20. Zhao X, Yamazaki D, Park KH, Komazaki S, Tjondrokoesoemo A, Nishi M, Lin P, Hirata Y, Brotto M, Takeshima H and Ma J. Ca2+ overload and sarcoplasmic reticulum instability in tric-a null skeletal muscle. J Biol Chem. 2010;285:37370–6. [PubMed: 20858894]

21. Yamazaki D, Komazaki S, Nakanishi H, Mishima A, Nishi M, Yazawa M, Yamazaki T, Taguchi R and Takeshima H. Essential role of the TRIC-B channel in Ca2+ handling of alveolar epithelial cells and in perinatal lung maturation. Development. 2009;136:2355–61. [PubMed: 19515693]
22. El-Ajouz S, Venturi E, Witschas K, Beech M, Wilson AD, Lindsay C, Eberhardt D, O'Brien F, Iida T, Nishi M, Takeshima H and Sitsapesan R. Dampened activity of ryanodine receptor channels in mutant skeletal muscle lacking TRIC-A. J Physiol. 2017;595:4769–4784. [PubMed: 28387457]
23. Su M, Gao F, Yuan Q, Mao Y, Li DL, Guo Y, Yang C, Wang XH, Bruni R, Kloss B, Zhao H, Zeng Y, Zhang FB, Marks AR, Hendrickson WA and Chen YH. Structural basis for conductance through TRIC cation channels. Nat Commun. 2017;8:15103. [PubMed: 28524849]
24. Ou X, Guo J, Wang L, Yang H, Liu X, Sun J and Liu Z. Ion- and water-binding sites inside an occluded hourglass pore of a trimeric intracellular cation (TRIC) channel. BMC Biol. 2017;15:31. [PubMed: 28431535]
25. Yang H, Hu M, Guo J, Ou X, Cai T and Liu Z. Pore architecture of TRIC channels and insights into their gating mechanism. Nature. 2016;538:537–541. [PubMed: 27698420]
26. Kasuya G, Hiraizumi M, Maturana AD, Kumazaki K, Fujiwara Y, Liu K, Nakada-Nakura Y, Iwata S, Tsukada K, Komori T, Uemura S, Goto Y, Nakane T, Takemoto M, Kato HE, Yamashita K, Wada M, Ito K, Ishitani R, Hattori M and Nureki O. Crystal structures of the TRIC trimeric intracellular cation channel orthologues. Cell Res. 2016;26:1288–1301. [PubMed: 27909292]
27. Lukyanenko V and Gyorke S. Ca2+ sparks and Ca2+ waves in saponin-permeabilized rat ventricular myocytes. J Physiol. 1999;521 Pt 3:575–85. [PubMed: 10601490]
28. Guo T, Nani A, Shonts S, Perryman M, Chen H, Shannon T, Gillespie D and Fill M. Sarcoplasmic reticulum K(+) (TRIC) channel does not carry essential countercurrent during Ca(2+) release. Biophys J. 2013;105:1151–60. [PubMed: 24010658]
29. Bers DM, Patton CW and Nuccitelli R. A practical guide to the preparation of Ca(2+) buffers. Methods Cell Biol. 2010;99:1–26. [PubMed: 21035681]
30. Picht E, Zima AV, Blatter LA and Bers DM. SparkMaster: automated calcium spark analysis with ImageJ. Am J Physiol Cell Physiol. 2007;293:C1073–81. [PubMed: 17376815]
31. Uehara A, Murayama T, Yasukochi M, Fill M, Horie M, Okamoto T, Matsuura Y, Uehara K, Fujimoto T, Sakurai T and Kurebayashi N. Extensive Ca2+ leak through K4750Q cardiac ryanodine receptors caused by cytosolic and luminal Ca2+ hypersensitivity. J Gen Physiol. 2017;149:199–218. [PubMed: 28082361]
32. Tang Y, Tian X, Wang R, Fill M and Chen SR. Abnormal termination of Ca2+ release is a common defect of RyR2 mutations associated with cardiomyopathies. Circ Res. 2012;110:968–77. [PubMed: 22374134]
33. Penner R, Neher E, Takeshima H, Nishimura S and Numa S. Functional expression of the calcium release channel from skeletal muscle ryanodine receptor cDNA. FEBS Lett. 1989;259:217–21. [PubMed: 2557244]
34. Takekura H, Takeshima H, Nishimura S, Takahashi M, Tanabe T, Flockerzi V, Hofmann F and Franzini-Armstrong C. Co-expression in CHO cells of two muscle proteins involved in excitation-contraction coupling. J Muscle Res Cell Motil. 1995;16:465–80. [PubMed: 8567934]
35. Ma J, Fill M, Knudson CM, Campbell KP and Coronado R. Ryanodine receptor of skeletal muscle is a gap junction-type channel. Science. 1988;242:99–102. [PubMed: 2459777]
36. Fill M, Coronado R, Mickelson JR, Vilven J, Ma J, Jacobson B and Louis CF. Abnormal ryanodine receptor channels in malignant hyperthermia. Biophysical Journal. 1990;57:471–475. [PubMed: 2306496]
37. Zhang Y I-TASSER server for protein 3D structure prediction. BMC Bioinformatics. 2008;9:40. [PubMed: 18215316]
38. Berman HM, Westbrook J, Feng Z, Gilliland G, Bhat TN, Weissig H, Shindyalov IN and Bourne PE. The Protein Data Bank. Nucleic acids research. 2000;28:235–242. [PubMed: 10592235]
39. Peng W, Shen H, Wu J, Guo W, Pan X, Wang R, Chen SR and Yan N. Structural basis for the gating mechanism of the type 2 ryanodine receptor RyR2. Science. 2016;354.
40. Pettersen EF, Goddard TD, Huang CC, Couch GS, Greenblatt DM, Meng EC and Ferrin TE. UCSF Chimera--a visualization system for exploratory research and analysis. J Comput Chem. 2004;25:1605–12. [PubMed: 15264254]

41. Huang SY, Yan C, Grinter SZ, Chang S, Jiang L and Zou X. Inclusion of the orientational entropic effect and low-resolution experimental information for protein-protein docking in Critical Assessment of PRedicted Interactions (CAPRI). Proteins. 2013;81:2183–91. [PubMed: 24227686]

42. Huang SY and Zou X. MDockPP: A hierarchical approach for protein-protein docking and its application to CAPRI rounds 15–19. Proteins. 2010;78:3096–103. [PubMed: 20635420]

43. Kolstad TR, van den Brink J, MacQuaide N, Lunde PK, Frisk M, Aronsen JM, Norden ES, Cataliotti A, Sjaastad I, Sejersted OM, Edwards AG, Lines GT and Louch WE. Ryanodine receptor dispersion disrupts Ca(2+) release in failing cardiac myocytes. Elife. 2018;7.

44. Liu Y, Wang R, Sun B, Mi T, Zhang J, Mu Y, Chen J, Bround MJ, Johnson JD, Gillis AM and Chen SR. Generation and characterization of a mouse model harboring the exon-3 deletion in the cardiac ryanodine receptor. PLoS One. 2014;9:e95615. [PubMed: 24743769]

45. Zhao YT, Valdivia CR, Gurrola GB, Powers PP, Willis BC, Moss RL, Jalife J and Valdivia HH. Arrhythmogenesis in a catecholaminergic polymorphic ventricular tachycardia mutation that depresses ryanodine receptor function. Proc Natl Acad Sci U S A. 2015;112:E1669–77. [PubMed: 25775566]

46. Pan Z, Hirata Y, Nagaraj RY, Zhao J, Nishi M, Hayek SM, Bhat MB, Takeshima H and Ma J. Co-expression of MG29 and ryanodine receptor leads to apoptotic cell death: effect mediated by intracellular Ca2+ release. J Biol Chem. 2004;279:19387–90. [PubMed: 15039443]

47. Jones PP, Jiang D, Bolstad J, Hunt DJ, Zhang L, Demaurex N and Chen SR. Endoplasmic reticulum Ca2+ measurements reveal that the cardiac ryanodine receptor mutations linked to cardiac arrhythmia and sudden death alter the threshold for store-overload-induced Ca2+ release. Biochem J. 2008;412:171–8. [PubMed: 18092949]

48. Curran J, Hinton MJ, Rios E, Bers DM and Shannon TR. Beta-adrenergic enhancement of sarcoplasmic reticulum calcium leak in cardiac myocytes is mediated by calcium/calmodulin-dependent protein kinase. Circ Res. 2007;100:391–8. [PubMed: 17234966]

49. Shannon TR, Ginsburg KS and Bers DM. Quantitative assessment of the SR Ca2+ leak-load relationship. Circ Res. 2002;91:594–600. [PubMed: 12364387]

50. Yang H, Hu M, Guo J, Ou X, Cai T and Liu Z. Pore architecture of TRIC channels and insights into their gating mechanism. Nature. 2016.

51. Ogawa Y Role of ryanodine receptors. Crit Rev Biochem Mol Biol. 1994;29:229–74. [PubMed: 8001396]

52. Tanabe T, Beam KG, Adams BA, Niidome T and Numa S. Regions of the skeletal muscle dihydropyridine receptor critical for excitation-contraction coupling. Nature. 1990;346:567–9. [PubMed: 2165570]

53. Ogawa Y, Kurebayashi N and Murayama T. Ryanodine receptor isoforms in excitation-contraction coupling. Adv Biophys. 1999;36:27–64. [PubMed: 10463072]

54. Bhat MB, Zhao J, Takeshima H and Ma J. Functional calcium release channel formed by the carboxyl-terminal portion of ryanodine receptor. Biophys J. 1997;73:1329–36. [PubMed: 9284301]

55. Bhat MB, Zhao J, Zang W, Balke CW, Takeshima H, Wier WG and Ma J. Caffeine-induced release of intracellular Ca2+ from Chinese hamster ovary cells expressing skeletal muscle ryanodine receptor. Effects on full-length and carboxyl-terminal portion of Ca2+ release channels. J Gen Physiol. 1997;110:749–62. [PubMed: 9382901]

56. Huang SY and Zou X. An iterative knowledge-based scoring function for protein-protein recognition. Proteins. 2008;72:557–79. [PubMed: 18247354]

57. Yan Z, Bai X-c, Yan C, Wu J, Li Z, Xie T, Peng W, Yin C-c, Li X, Scheres SHW, Shi Y and Yan N. Structure of the rabbit ryanodine receptor RyR1 at near-atomic resolution. Nature. 2014;517:50. [PubMed: 25517095]

58. Tae H, Wei L, Willemse H, Mirza S, Gallant EM, Board PG, Dirksen RT, Casarotto MG and Dulhunty A. The elusive role of the SPRY2 domain in RyR1. Channels (Austin). 2011;5:148–60. [PubMed: 21239886]

59. Liu Y, Wei J, Wong King Yuen SM, Sun B, Tang Y, Wang R, Van Petegem F and Chen SRW. CPVT-associated cardiac ryanodine receptor mutation G357S with reduced penetrance impairs

Ca2+ release termination and diminishes protein expression. PLoS One. 2017;12:e0184177. [PubMed: 28961276]

60. Zvaritch E, Depreux F, Kraeva N, Loy RE, Goonasekera SA, Boncompagni S, Kraev A, Gramolini AO, Dirksen RT, Franzini-Armstrong C, Seidman CE, Seidman JG and Maclennan DH. An Ryr1I4895T mutation abolishes Ca2+ release channel function and delays development in homozygous offspring of a mutant mouse line. Proc Natl Acad Sci U S A. 2007;104:18537–42. [PubMed: 18003898]
61. Thomas NL, Lai FA and George CH. Differential Ca2+ sensitivity of RyR2 mutations reveals distinct mechanisms of channel dysfunction in sudden cardiac death. Biochem Biophys Res Commun. 2005;331:231–8. [PubMed: 15845383]
62. Savio-Galimberti E and Knollmann BC. Channel Activity of Cardiac Ryanodine Receptors (RyR2) Determines Potency and Efficacy of Flecainide and R-Propafenone against Arrhythmogenic Calcium Waves in Ventricular Cardiomyocytes. PLoS One. 2015;10:e0131179. [PubMed: 26121139]
63. Ullrich ND, Valdivia HH and Niggli E. PKA phosphorylation of cardiac ryanodine receptor modulates SR luminal Ca2+ sensitivity. J Mol Cell Cardiol. 2012;53:33–42. [PubMed: 22487381]
64. Smith GL and O'Neill SC. A comparison of the effects of ATP and tetracaine on spontaneous Ca(2+) release from rat permeabilised cardiac myocytes. J Physiol. 2001;534:37–47. [PubMed: 11432990]
65. Peralvarez-Marin A, Tae H, Board PG, Casarotto MG, Dulhunty AF and Samso M. 3D Mapping of the SPRY2 domain of ryanodine receptor 1 by single-particle cryo-EM. PLoS One. 2011;6:e25813. [PubMed: 21998699]
66. MacLennan DH and Chen SR. Store overload-induced Ca2+ release as a triggering mechanism for CPVT and MH episodes caused by mutations in RYR and CASQ genes. J Physiol. 2009;587:3113–5. [PubMed: 19567749]
67. Gillespie D and Fill M. Intracellular calcium release channels mediate their own countercurrent: the ryanodine receptor case study. Biophys J. 2008;95:3706–14. [PubMed: 18621826]
68. Zsolnay V, Fill M and Gillespie D. Sarcoplasmic Reticulum Ca(2+) Release Uses a Cascading Network of Intra-SR and Channel Countercurrents. Biophys J. 2018;114:462–473. [PubMed: 29401443]
69. Zima AV and Blatter LA. Inositol-1,4,5-trisphosphate-dependent Ca(2+) signalling in cat atrial excitation-contraction coupling and arrhythmias. J Physiol. 2004;555:607–15. [PubMed: 14754996]
70. Domeier TL, Zima AV, Maxwell JT, Huke S, Mignery GA and Blatter LA. IP3 receptor-dependent Ca2+ release modulates excitation-contraction coupling in rabbit ventricular myocytes. Am J Physiol Heart Circ Physiol. 2008;294:H596–604. [PubMed: 18055509]
71. Kockskamper J, Zima AV, Roderick HL, Pieske B, Blatter LA and Bootman MD. Emerging roles of inositol 1,4,5-trisphosphate signaling in cardiac myocytes. J Mol Cell Cardiol. 2008;45:128–47. [PubMed: 18603259]
72. Li X, Zima AV, Sheikh F, Blatter LA and Chen J. Endothelin-1-induced arrhythmogenic Ca2+ signaling is abolished in atrial myocytes of inositol-1,4,5-trisphosphate(IP3)-receptor type 2-deficient mice. Circ Res. 2005;96:1274–81. [PubMed: 15933266]
73. Zhang WM, Lin MJ and Sham JS. Endothelin-1 and IP3 induced Ca2+ sparks in pulmonary arterial smooth muscle cells. J Cardiovasc Pharmacol. 2004;44 Suppl 1:S121–4. [PubMed: 15838259]
74. Zhang WM, Yip KP, Lin MJ, Shimoda LA, Li WH and Sham JS. ET-1 activates Ca2+ sparks in PASMC: local Ca2+ signaling between inositol trisphosphate and ryanodine receptors. Am J Physiol Lung Cell Mol Physiol. 2003;285:L680–90. [PubMed: 12740215]
75. Tjondrokoesoemo A, Li N, Lin PH, Pan Z, Ferrante CJ, Shirokova N, Brotto M, Weisleder N and Ma J. Type 1 inositol (1,4,5)-trisphosphate receptor activates ryanodine receptor 1 to mediate calcium spark signaling in adult mammalian skeletal muscle. J Biol Chem. 2013;288:2103–9. [PubMed: 23223241]

NOVELTY AND SIGNIFICANCE

What Is Known?

- Dysfunction of ryanodine receptor (RyR)-mediated Ca^{2+} signaling contributes to arrhythmia and heart failure.
- TRIC channels provide counter-current movement during Ca^{2+} release from intracellular stores.
- Crystal structure of TRIC lacking the carboxyl-terminal tail (CTT) domain has been solved.

What New Information Does This Article Contribute?

- TRIC-A knockout mouse heart shows abnormal response to isoproterenol stimulation due to dysfunctional Ca^{2+} signaling.
- TRIC-A interacts with RyR to directly control Ca^{2+} release in cardiomyocytes.

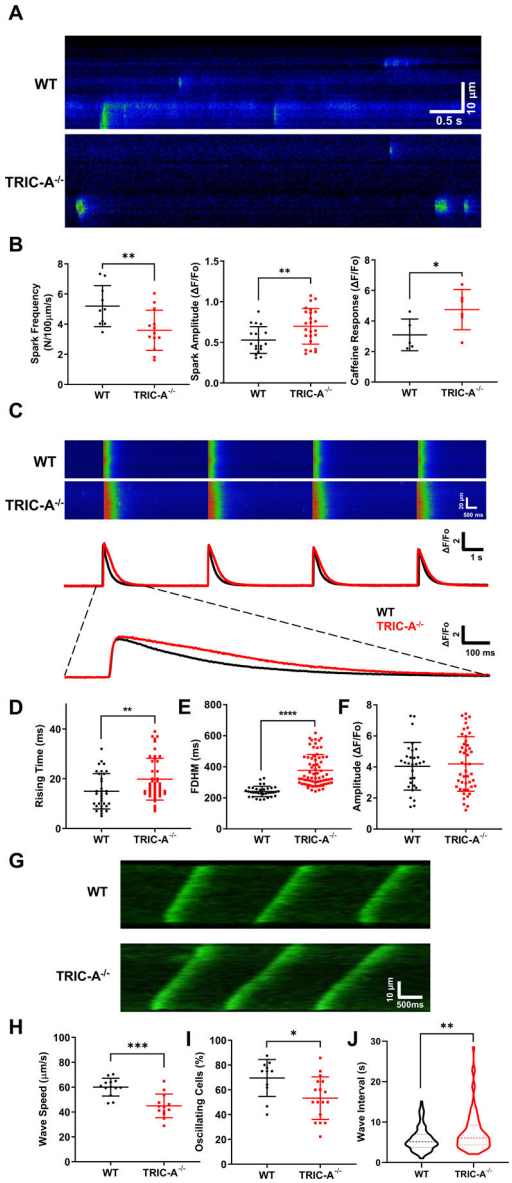

Fig. 1. Compromised Ca^{2+} signaling in cardiomyocytes derived from TRIC-$A^{-/-}$ mice.

A. Confocal line scan images of Ca^{2+} sparks in isolated cardiomyocytes from WT and TRIC-$A^{-/-}$ mice, after pacing by 0.5 Hz of electric field stimulation for 20 s. **B**. Ca^{2+} spark amplitude was higher (p=0.0091, 2-tailed t-test) and spark frequency was lower (p=0.0098, 2-tailed t-test) in TRIC-$A^{-/-}$ cardiomyocytes, compared with WT cardiomyocytes. Caffeine-induced Ca^{2+} release was significantly higher (p=0.0487, 2-tailed t-test) in TRIC-$A^{-/-}$ cardiomyocytes. **C**. Line-scan imaging of electric pacing induced intracellular Ca^{2+} transients, demonstrating the different patterns in WT and TRIC-$A^{-/-}$ cardiomyocytes. Data from individual cardiomyocytes were plotted. Rising time (**D**) (P=0.0090, 2-tailed t-test), full-duration-half-maximum (FDHM) (**E**) (P= <0.0001, Mann-Whitney test), and peak amplitude of electric pacing induced Ca^{2+} transients (**F**) (P=0.7473, Mann-Whitney test) are plotted for TRIC-$A^{-/-}$ (red) and WT (black) cardiomyocytes. **G**. Different propagating patterns of store-overload induced Ca^{2+} waves in WT and TRIC-$A^{-/-}$ cardiomyocytes.

Speed of Ca^{2+} wave propagation (H) (P=0.0001, 2-tailed t-test), percentage of oscillating cells (**I**) (p=0.0205, 2-tailed t-test), and interval between Ca^{2+} waves (**J**) (n=165 for WT, n=89 for TRIC-$A^{-/-}$, p=0.0047, Mann-Whitney test) were significantly larger in TRIC-$A^{-/-}$ cardiomyocytes. * P<0.05, ** P<0.01, **** P<0.0001.

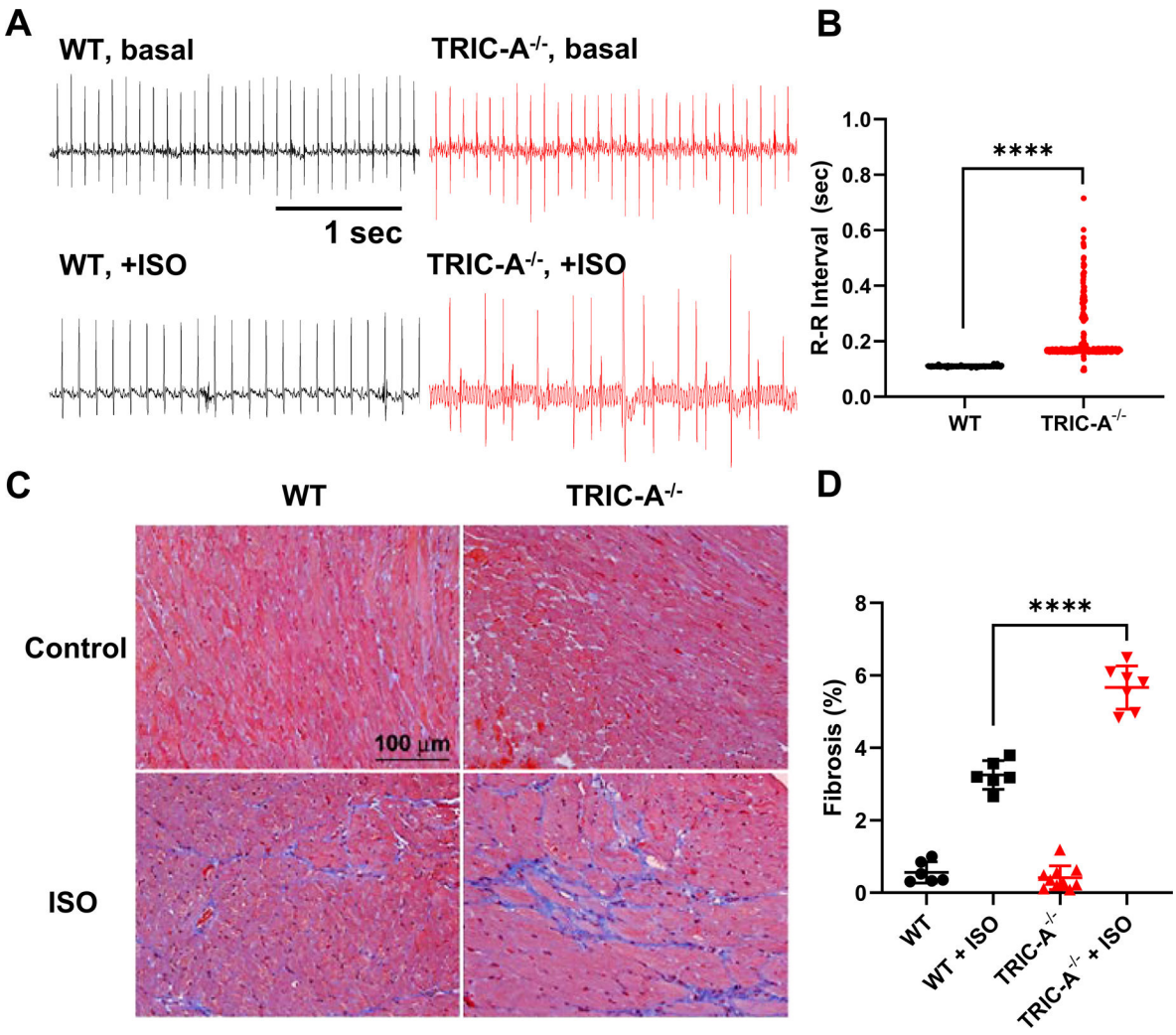

Fig. 2. Irregular ECG and increased cardiac fibrosis in TRIC-A$^{-/-}$ mice upon stimulation with isoproterenol.

A. Representative traces of ECG in WT and TRIC-A$^{-/-}$ mice before and after treatment of ISO. **B**. Distribution of ECG R-R intervals at 1 hr after 80 mg/kg ISO injection. ($P<0.0001$, Mann-Whitney test) **C**. Trichrome stain of WT and TRIC-A$^{-/-}$ heart at 2 weeks after treatment of PBS or ISO (60 mg/kg/day). **D**. Summary data with percentage of fibrosis area in WT and TRIC-A$^{-/-}$ heart stained by Mason's trichrome ($P<0.001$ across the groups, ANOVA test; WT+ISO vs TRIC-A$^{-/-}$+ISO: $P<0.0001$, Tukey's test).

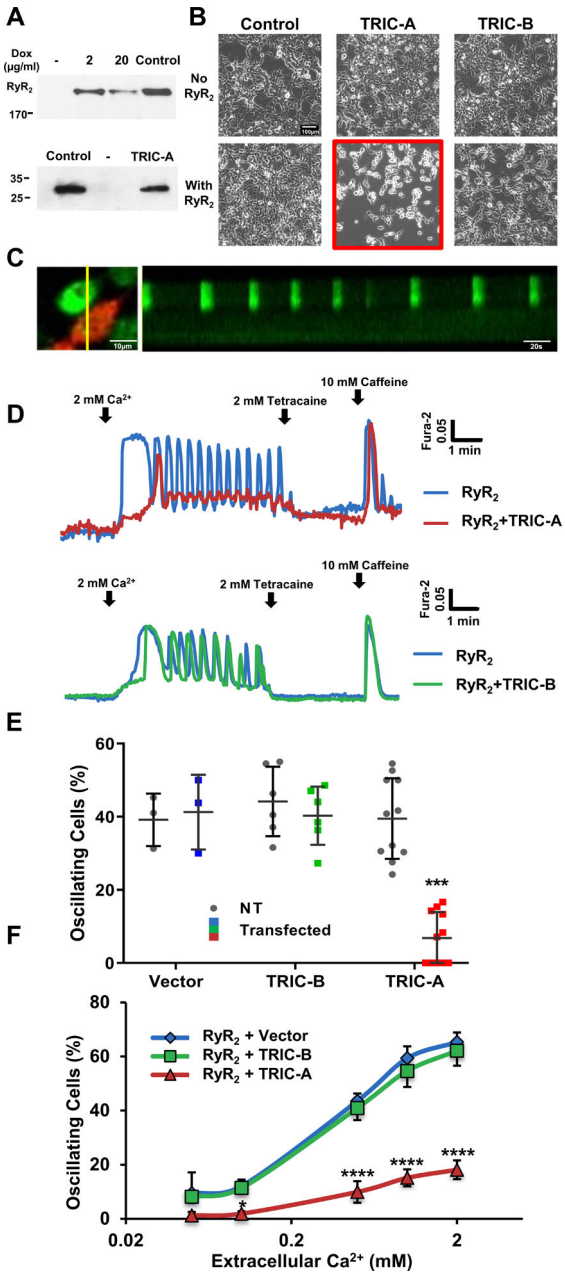

Fig. 3. Effect of TRIC-A and TRIC-B on RyR_2-mediated SOICR in HEK293 cells.

A. Western blot of RyR_2 and TRIC-A in HEK293 cells with tetracycline-inducible expression of RyR_2. Mouse heart lysate was used as positive control of RyR_2 and TRIC-A expression. B. Representative images of HEK293 cells without RyR_2 expression (top) and with RyR_2 expression (bottom). Following baculovirus infection, only cells co-expressing RyR_2 and TRIC-A became round and detached from the plate (middle-bottom panel). Co-expression of RyR_2 and TRIC-B had no effect on cell viability. Scale bar, 200 μm. **C**. Line-scan image of Ca^{2+} oscillation, representing SOICR, in HEK293 cells expressing RyR_2 alone (non-red cell) and lack of Ca^{2+} oscillation in HEK293 cells co-expressing RyR_2 and TRIC-A (red cell). **D**. Representative Fura-2 Ca^{2+} measurement in HEK293 cells with stable

expression of RyR_2 (blue trace), co-expression of TRIC-A and RyR_2 (red trace), and co-expression of TRIC-B and RyR_2 (green trace). **E**. Summary data with percentage of cells showing spontaneous Ca^{2+} oscillations in 0.5mM Ca^{2+}. (P=0.0003 across groups, 2-way ANOVA; TRIC-A vs NT: P<0.0001, Sidak's test). **F**. Co-expression of TRIC-A and RyR_2 alters the dependence of SOICR on extracellular Ca^{2+} concentration. Co-expression of TRIC-B and RyR_2 produced similar response of SOICR with changes of $[Ca]_o$, as cells transfected with pCMS-RFP vector control. Data from 4 individual experiments were used for the statistical analyses. (P<0.0001 across groups, 2-way ANOVA; RyR_2+TRIC-A vs RyR_2+TRIC-B: P<0.0001, Sidak's test) ****P<0.0001.

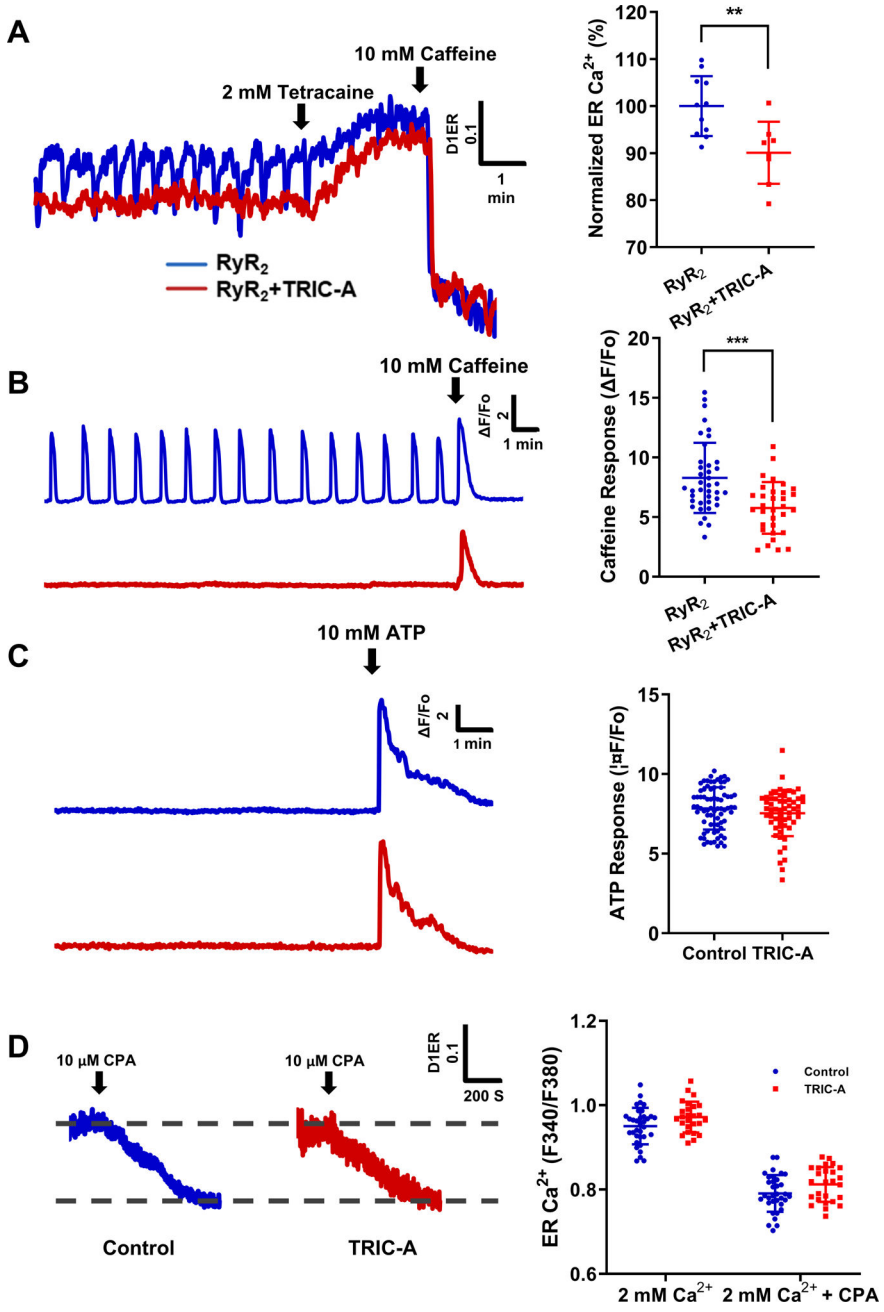

Fig. 4. Effect of TRIC-A on changes in ER Ca^{2+} load require interaction with RyR_2.

A. ER luminal Ca^{2+} measured by D1ER in cells expressing RyR_2 (*blue*), or RyR_2 + TRIC-A (*red*). 2 mM tetracaine inhibited ER Ca^{2+} oscillations and increased ER Ca^{2+} store and 10 mM caffeine caused depletion of ER Ca^{2+} store. (P=0.0042, 2-tailed t-test) **B**. Caffeine induced Ca^{2+} release from the ER store in cells expressing RyR_2 alone (*blue*) and in cells with co-expression of TRIC-A and RyR_2 (*red*) (p=0.0001, 2-tailed t-test) . **C**. Cytosolic Ca^{2+} release by ATP in HEK293 cells without RyR_2 expression showed similar response with or without TRIC-A expression. (P=0.2667, Mann-Whitney test) **D**. D1ER measurement of CPA (SERCA inhibitor) treatment showed that TRIC-A overexpression did not affect the total ER

Ca^{2+} and the ER Ca^{2+} uptake in HEK293 cells (2 mM Ca^{2+}: P=0.2627; 2 mM Ca^{2+}+CPA: P=0.2695, 2-way ANOVA, Sidak's test).

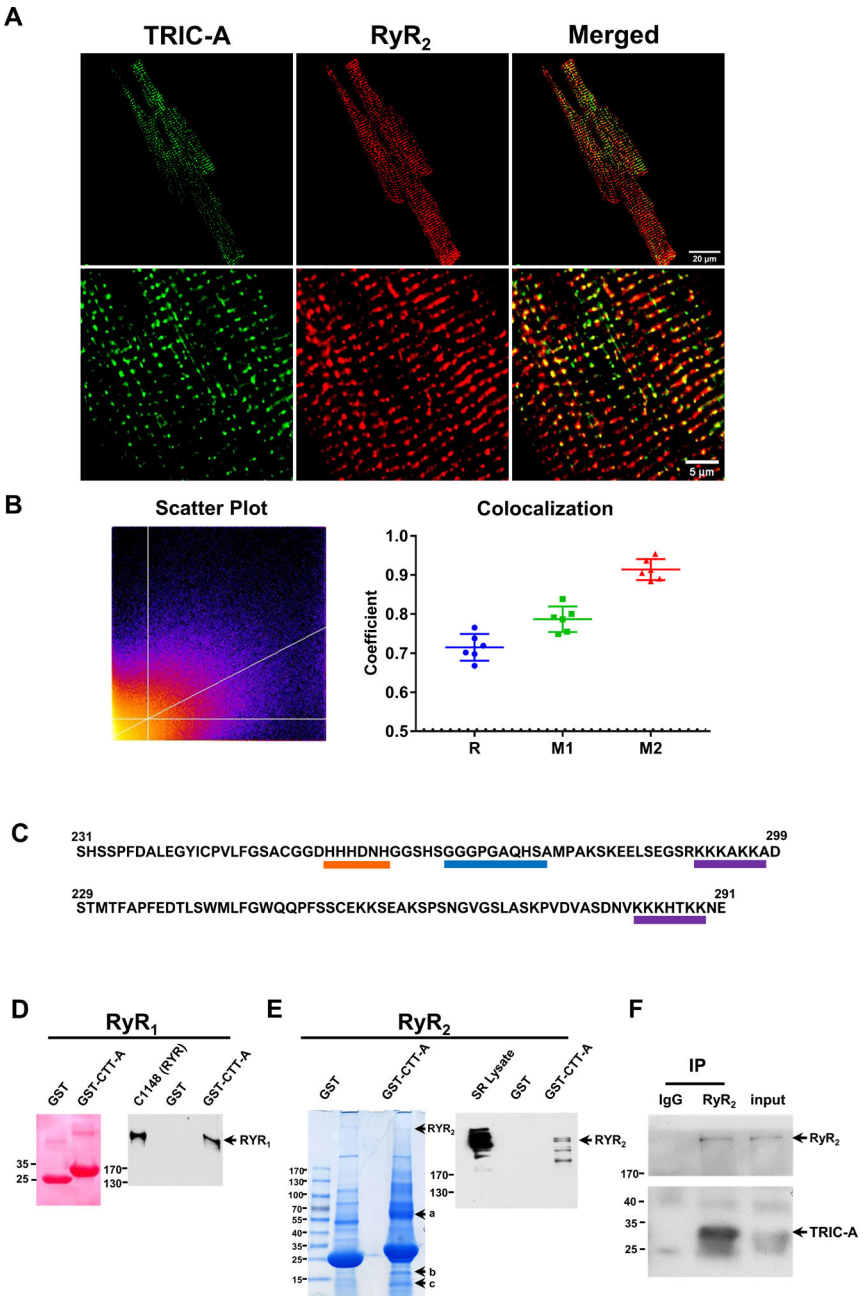

Fig. 5. Co-localization of TRIC-A and RyR_2 in mouse cardiomyocytes and CTT-A interaction with RyR.

A. Fluorescent staining shows TRIC-A and RyR_2 are highly co-localized together in mouse isolated cardiomyocytes. **B**. Images were analyzed by scatter plot, Pearson coefficient (R) and Mander's coefficient (M1 and M2). Bright yellow color of the scatterplot across the line indicates stronger co-localization. A value of 1 for R, M1/M2 indicates perfect co-localization and 0 indicates no co-localization; a threshold of 0.5 usually indicates good co-localization. M1 represents the degree of green fluorescence (TRIC-A) overlay with red fluorescence (RyR_2); M2 represents the degree of red fluorescence overlay with green fluorescence. **C**. CTT-A and CTT-B diverge from each other. CTT-A contains a histidine-

rich motif (orang) and a polylysine domain (purple), which are flanked by a hydrophobic domain (blue). Such structure is similar to the intracellular-loop joining repeats II and III of the L-type Ca^{2+} channel. Only the polylysine domain is present in CTT-B. **D**. GST-CTT-A can pull down RyR_1 from C1148 cells. **E**. GST-CTT-A can pull down RyR_2 from SR vesicle isolated from rat heart, and three other candidate proteins (labeled as a, b and c.). Western blot confirmed the pull-down of RyR_2 from heart SR vesicle. GST alone does not pull down RyR_2. **F**. TRIC-A could be immuno-precipitated with RyR_2 in HEK293 cells co-expressing RyR_2 and TRIC-A.

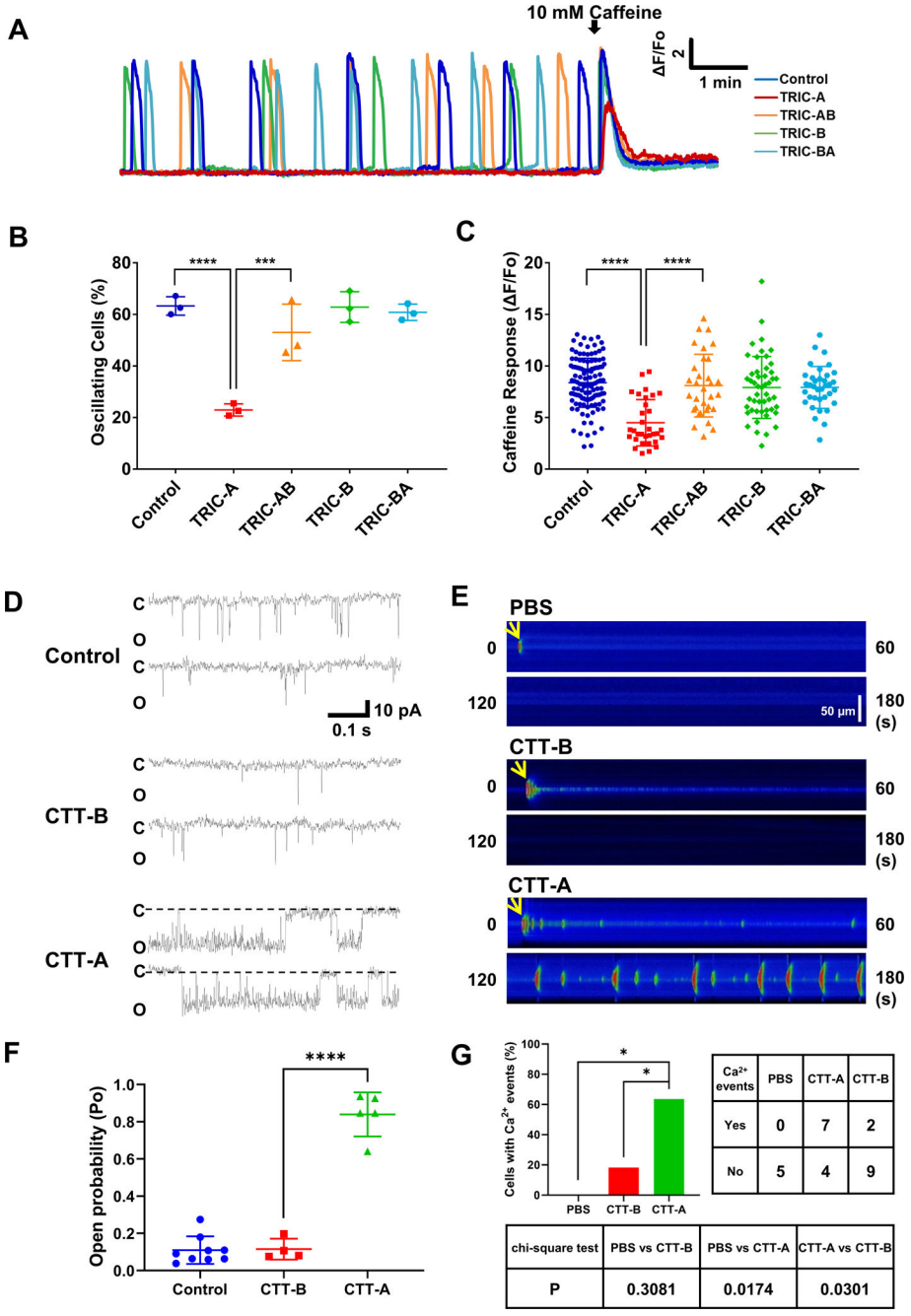

Fig 6. CTT-A directly modulates RyR_2 channel function.

A. TRIC-A, TRIC-B, TRIC-AB and TRIC-BA were transiently transfected into HEK293 cells with stable expression of RyR_2. Represent traces of spontaneous Ca^{2+} oscillations in 2 mM Ca^{2+} were shown. **B**. Percentage of cells with SOICR was quantified. (P<0.0001 across groups, ANOVA; Control vs TRIC-A: P<0.0001; TRIC-A vs TRIC-AB: P=0.0009, Tukey's test) **C**. Caffeine-induced Ca^{2+} release was used to quantify the impact of the various TRIC-A and TRIC-B constructs on ER Ca^{2+} stores. (P<0.001 for Kruskal-Wallis test for whole group; TRIC-A vs TRIC-AB: P<0.0001, TRIC-A vs Control: P<0.0001, Dunn's test). **D**. Reconstitution of RyR_2 channels in lipid bilayer. Single channel activity was measured with

250 mM Cs (cis)/50 mM Cs (trans) and 1 μM free Ca^{2+} in the cis solution. Holding potential was −60 mV. Open probability of individual channels was calculated from a continuous recording of 5 min, and data from multiple measurements were averaged. Addition of 1 μM CTT-A to cis solution led to significant increase in the bursting pattern of RyR_2 channel, whereas addition of 10 μM TRIC-B-tail did not affect RyR_2 activity. **E**. Confocal line scan images of Ca^{2+} events measured by Fluo-4 after microinjection of CTT-A or CTT-B into isolated cardiomyocytes. **F**. Statistical analysis of RyR_2 channel open probabilities. ($P<0.0001$ across groups, ANOVA; TRIC-A vs Control: $P<0.0001$, TRIC-A vs TRIC-B: $P<0.0001$, Tukey's test) **G**. CTT-A induced significantly more Ca^{2+} release events in cardiomyocytes than CTT-B and PBS does. (CTT-A vs PBS: $P=0.0174$; CTT-A vs CTT-B: $P=0.0301$, chi-square test)

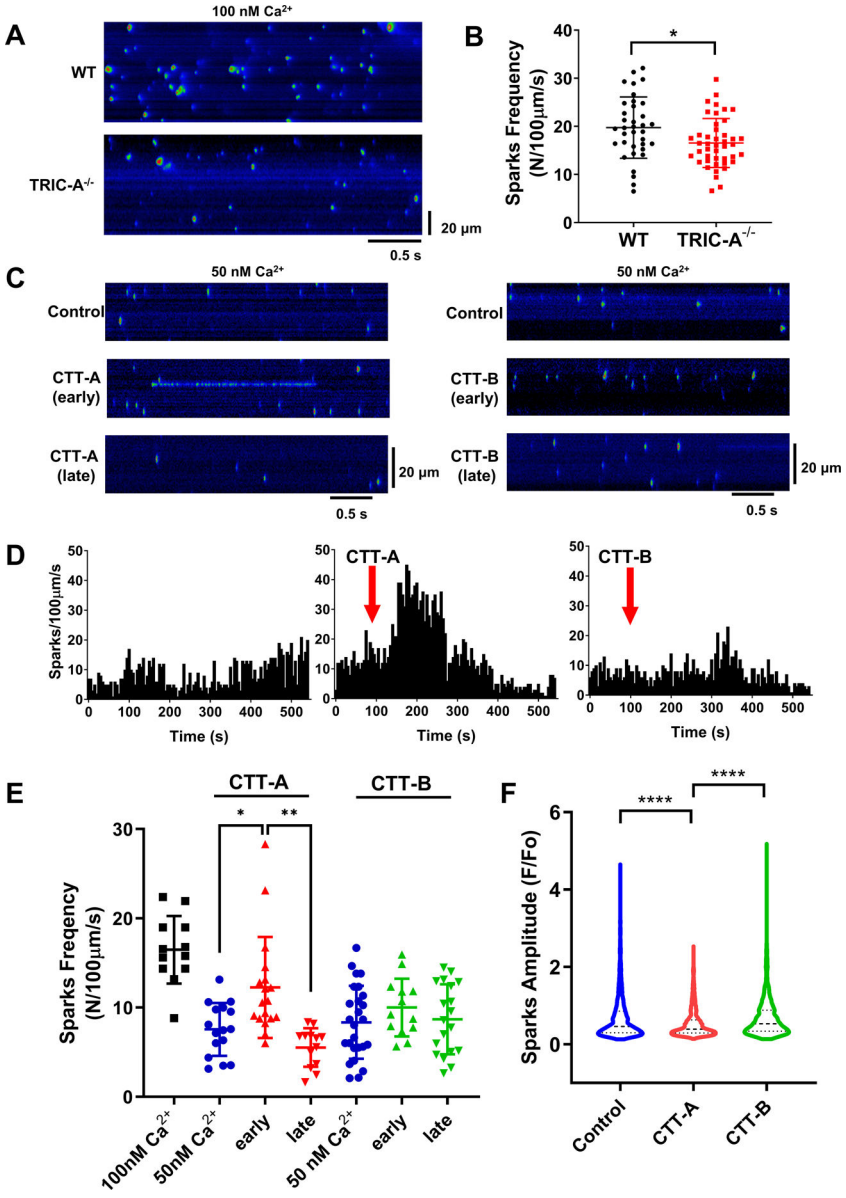

Fig. 7. CTT-A enhances Ca^{2+} spark activities in permeabilized TRIC-$A^{-/-}$ cardiomyocytes.

A. Line-scan images of Ca^{2+} sparks in saponin-permeabilized wild type (top) and TRIC-A $^{-/-}$ cardiomyocytes (bottom). **B**. Dot plot of spontaneous Ca^{2+} spark activities in wild type and TRIC-A cardiomyocytes at 100 nM free cytosolic Ca^{2+}. (P =0.0147, 2-tailed t-test) . **C**. Left panel shows distinct streaming-pattern of Ca^{2+} sparks observed in TRIC-$A^{-/-}$ cardiomyocytes following 1 min application of 10 μM CTT-A (early), with apparent suppression of Ca^{2+} sparks at 5 min after CTT-A treatment (late). Treatment with CTT-B (10 μM) did not induce measurable changes in Ca^{2+} spark activity (*right panels*). All Ca^{2+} sparks were measured with a cytosolic solution containing 50 nM free Ca^{2+}. **D**. Diary plots of Ca^{2+} spark activities under control condition of 50 nM free Ca^{2+} (left), with addition of CTT-A (middle) and CTT-B (right). **E**. Scattered plots of Ca^{2+} spark events from individual cardiomyocytes. Two separate groups of experiments were performed with CTT-A and CTT-

B, all with cytosolic free Ca^{2+} buffered at 50 nM. Early – indicates 0–3 min following CTT-A/B treatment; late – indicates 3–6 min following CTT-A/B treatment. ($P<0.0001$ across groups, ANOVA; 50nM Ca^{2+} vs early: $P=0.0130$, early vs late: $P=0.0002$, Tukey's test) **F**. Averaged value of Ca^{2+} spark amplitudes measured at 50 nM free cytosolic Ca^{2+} (Control, blue, n=3939), with early addition of CTT-A (red, n=3434) or CTT-B (green, n=2126). ($P<0.0001$ for ANOVA test; $P<0.0001$, CTT-A vs Control, CTT-A vs CTT-B, Tukey's test) **P<0.001, ****P<0.0001

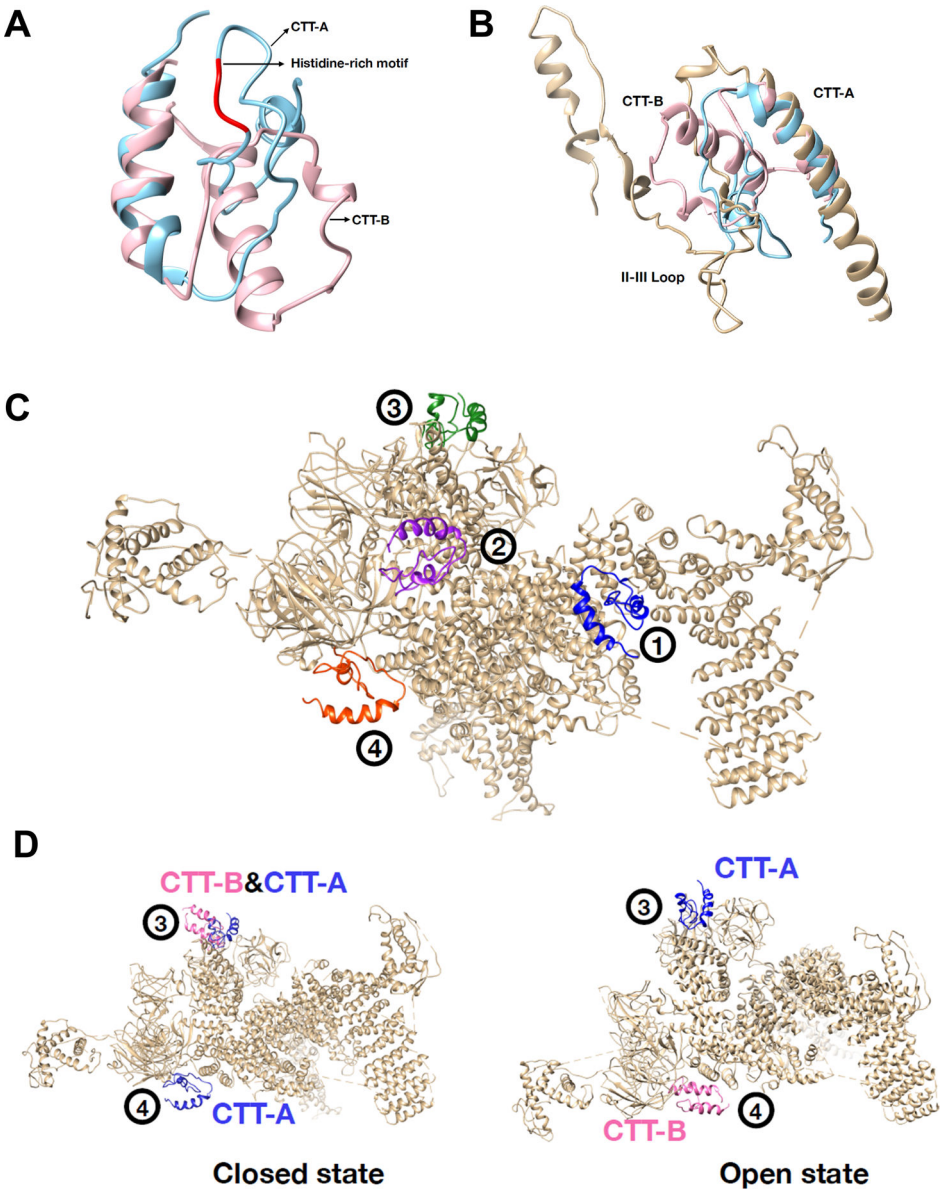

Fig. 8. Docking of CTT-A and CTT-B with open and closed-state of the RyR_2 channel.

A. Structural comparison between CTT-A (cyan) and CTT-B (pink) in ribbon representation. The histidine-rich motif in CTT-A is colored red. **B**. Structural comparison of CTT-A, CTT-B and the II-III loop of DHPR. **C**. Four potential binding sites of CTT-A interaction with $hRyR_2$ were predicted from molecular docking. Both $hRyR_2$ (grey) and CTT-A are plotted in ribbon representation. CTT-A is colored differently at the four sites. **D**. CTT-A and CTT-B bind to $hRyR_2$ distinctively on Site 3 and Site 4. Left - binding to the closed structure of $hRyR_2$; right - binding to the open structure of $hRyR_2$. CTT-A (blue), CTT-B (pink) and $hRyR_2$ (grey) are plotted in ribbon representation.